Impacts of environmental pollution on mangrove phenology: Combining remotely sensed data and generalized additive models.

Celis-Hernandez, Omar[ab]; Villoslada-Peciña, Miguel[cd]; Ward, Raymond D.[ce]; Bergamo, T.F.[c]; Perez-Ceballos Rosela[ab]; Girón-García María Patricia[f].

[a]Instituto de Ciencias del Mar y Limnología, Universidad Nacional Autónoma de México, Estación el Carmen, Campeche, C.P. 24157, Ciudad del Carmen, México.

[b]Dirección de Cátedras CONACYT. Av. Insurgentes Sur 1582, Alcaldía Benito Juárez, C.P. 03940, Ciudad de México.

[c]Institute of Agriculture and Environmental Sciences, Estonian University of Life Sciences, Kreutzwaldi 5, EE-51014 Tartu, Estonia

[d]Department of Geographical and Historical Studies, University of Eastern Finland, P.O. Box 111, 80101, Joensuu, Finland

[e]Centre for Aquatic Environments, University of Brighton, Cockcroft Building, Moulsecoomb, Brighton, BN2 4GJ, United Kingdom.

[f]Laboratorio de Fluorescencia de Rayos X. LANGEM. Instituto de Geología, Universidad Nacional Autónoma de México; Circuito Exterior, Ciudad Universitaria, Coyoacan, C.P. 04510, Ciudad de México, México.

*Corresponding author
Email address: celis0079@yahoo.es

Highlights

- Sentinel-2 data, HANTS and GAMs are used to detect phenology trends in mangroves
- Models show phenology shifts as a response to environmental variables and trace elements
- Pb and Cu lead to delays in the start of the season
- Future research should address long-term effects of pollution on phenology

Abstract

Mangrove ecosystems worldwide have been affected by anthropogenic activities that modify natural conditions and supply trace elements that affect mangrove health and development. In order to gain a better understanding of these ecosystems, and assess the influence of physicochemical (granulometry, pH, salinity and ORP) and geochemical variables (concentrations of V, Cr, Co, Ni, Cu, Zn, Pb, Rb, Sr and Zr) on mangrove phenology, we combined field and satellite derived remotely sensed data. Phenology metrics in combination with Generalized Additive Models showed that start of the season was strongly influenced by Pb and Cu pollution as well as salinity and pH, with a large percentage of deviance explained (92.10%) by the model. Start of season exhibited non-linear delays as a response to pollution. Other phenology parameters such as the length of season, timing of the peak of season, and growth peak also indicated responses to both trace elements and physicochemical and geochemical variables, with percentages of deviance explained by the models ranging between 33.90% and 97.70%. While the peak of season showed

delays as a response to increased pH and decreased salinity, growth peak exhibited a non-linear decrease as a response to increased Sr concentrations. These results suggest that trace element pollution is likely to lead to altered phenological patterns in mangroves.

Keywords: Trace elements, remote sensing, mangrove phenology, Gulf of Mexico.

1. Introduction

Mangroves provide a wide range of ecosystem services that support some of the poorest communities worldwide such as East, West and South Africa, the Sundarbans between India and Bangladesh or regions of Central and South America (Ward et al., 2016). Ecosystem services include: protection from flooding, storm surges, and erosion, supporting commercially important fish and bivalve species, carbon sequestration and storage, and estuarine filtration and storage of contaminants (Huxham et al., 2017; Celis et al., 2020; Lacerda et al., 2021). In urban mangroves, where ecosystem service provision is often diminished as a result of direct or indirect anthropogenic pressures (Veettil et al., 2018), how they are responding to global pressures is often uncertain (Turschwell et al., 2020). The filtration, sequestration and storage of contaminants, such as trace elements, is an important ecosystem service provided by mangroves, and is particularly acute in urban mangroves, whether from wastewater treatment plants (WWTP), aqua/agricultural inputs, urban run-off, or industrial activity (Celis et al., 2020; Pinheiro et al., 2021; Lacerda et al., 2021). This is likely to have an influence on ecosystem function, through leaf loss, altered structure of the trees, reduced canopy, and in extreme cases tree mortality (Arrivabene et al., 2015; Capdeville et al., 2018; Connolly et al., 2020). Environmental stressors have been shown to impact mangrove phenology (Pastor-Guzman et al., 2018; Songsom et al., 2020). However, there has been little research conducted on the impacts of environmental pollution on mangrove phenology.

Mangrove vegetation phenology studies have adopted a wide range of methods in recent decades, from field observations of phenology events such as flowering and fruiting (de Lima Nadia et al., 2012) to digital repeat photography or phenocams (Songsom et al., 2021). Satellite-based vegetation phenology has also emerged as a tool to address larger geographical scales. These phenology studies rely on models to interpolate a time series of vegetation indices and reveal the timing of seasonal biological events associated with plant phenology (Younes et al., 2021). Many of these studies take advantage of the ability of satellite-derived vegetation indices to detect variations in the spectral characteristics of vegetation as a response to environmental change. In addition, the temporal resolution of satellite missions such as Sentinel-2 (5-10 days revisit time) or Landsat (8-16 days revisit time) enables the detection of phenological trends throughout one year (Vrieling et al., 2018) or multiple decades (Garonna et al., 2016). While most of these models can detect subtle phenological changes (Rodriguez-Galiano at el., 2015, Zeng et al., 2020), mangroves pose a challenge, as litterfall and replacement of old leaves occurs continuously throughout the season (Pastor-Guzman et al., 2018), leading to attenuated phenology spectral-temporal profiles.

Several satellite-based mangrove phenology studies published in the past few years take advantage of the cloud computing capabilities of Google Earth Engine (Gorelick et al., 2017). For instance, Li et al. (2019) used Sentinel-2 imagery to model the phenological trajectories of different mangrove species in China. Similarly, Valderrama-Landeros et al. (2021) computed Sentinel-2 phenology series in Google Earth Engine in order to better discriminate mangrove species in semi-arid mangroves in Mexico. The availability of continuous, multi-decadal satellite imagery such as the Landsat program has also opened a realm of possibilities in mangrove research (Younes et al., 2017). Some studies have used Landsat time series to detect change and regeneration events in mangroves over several decades (Otero et al., 2019, Chamberlain et al., 2021), while others have used the long-term data series to unveil phenology shifts (Songsom et al., 2019).

The rise in freely available medium to high resolution passive multi-spectral satellite derived data also provides an opportunity to undertake spatially explicit assessments of impacts of environmental stressors in mangrove ecosystems. Giri et al. (2011) documented the extent and status of mangroves in Louisiana, U.S., before and after an oil spill using Landsat satellite images. Likewise, Mandal and Hosaka (2020) quantified and mapped cyclone-induced changes in mangroves across Bangladesh and India over 3 decades. Beyond the number of satellite observations available at any given location, the high spatial resolution of currently active satellite missions (e.g., 10-20 m for Sentinel-2) could unveil the effects of point source pollution in relatively small regions. Satellite imagery has been previously used to detect the impact of various pollution sources, from oil spills in coastal vegetation (Balogun et al., 2020) to vegetation stress in urban environments (Cârlan et al., 2020).

Despite the wide use of remote sensing in mangrove phenology, no study to date has used satellite imagery to examine the effects of pollution on mangrove phenology. The present work aims to fill this knowledge gap and evaluate the influence of environmental variables, including trace element contamination, on mangrove phenology using satellite derived remotely sensed data. Specifically, two objectives are addressed in this study:

- To model phenology profiles of mangroves at Isla del Carmen (Mexico) using a time series of Sentinel-2 multispectral data.
- To assess the effects of environmental variables and trace element contamination on the timing and characteristics of mangrove phenology dynamics.

2. Materials and methods

2.1 Study site description

Isla del Carmen is the eighth largest island in Mexico (142 km^2 area) and is home to the second most populous city (248, 303 inhabitants) in Campeche State (INEGI, 2018). On the south coast of the island fluvial discharges supply nutrients, sediments, as well as pollutants generated by agriculture, cattle and other human activities (Carvalho et al., 2009), while on the north coast the marine environment dominates and houses the Cantarell oil field, which is the largest producer of gas (38%) and offshore oil (56.5%) in Mexico (Nava-Fuentes et al., 2018; PEMEX, 2018). The weather is generally warm with summer rainfall. The average annual temperature and rainfall are 26.7°C and 1900 mm, ranging between 23.9°C and 28.8°C, and 1174 mm and 3139 mm respectively. Seasonally, three different regimes are recognizable, the dry season (Feb-May), rainy season (Jun-Sep), and stormy season (Oct-Jan).

Mangrove ecosystems of Isla del Carmen are situated in the Wildlife Protection Area Laguna de Terminos, which includes the largest coastal lagoon environment in Mexico (about 7050 km^2) (INEGI,

2018) (Figure 1). Historically, mangroves from Isla del Carmen have experienced a reduction in extent due to the urban expansion of Ciudad del Carmen. Nowadays, the urban area covers 23% of the island, while the remaining 77% is still covered by mangroves that are distributed according to topography and tidal influence (Perez et al., 2020). The main mangrove species distributed around the Island are red mangrove (*Rhizophora mangle* L.), buttonwood mangrove (*Conocarpus erectus*), black mangrove (*Avicennia germinans*), and white mangrove (*Laguncularia racemosa*) (Canales et al., 2019). However, in the urban adjacent mangroves, *Conocarpus erectus* and *Rhizophora mangle* dominate.

2.2 Sampling and clustering of study sites

Field data were collected in August 2019 from thirty-six mangrove sites on Isla del Carmen (Figure 1). Physicochemical parameters such as pH, salinity and ORP in seawater were measured in situ at all sites with a YSI Pro multiparameter sonde at the same time as sediment samples were collected. This equipment was calibrated with standard solutions before use to ensure physicochemical data quality.

Following the gradient of anthropogenic influence across the island (Figure 1) a total of thirty-six sediment samples were collected. Sediments were collected using a Van Veen dredge sampler at a water depth of 0.5-2.5m between mid and high tide and were stored in plastic bags at 4°C until analysed. During sampling, sediment samples were taken from the middle of the dredge with a plastic spatula to avoid any trace element contamination by contact with metallic parts from the dredge, and with the purpose to take the most recently deposited sediment, the first centimetre of the surface sediment was collected.

In the laboratory, samples were split in two halves, one half was used for granulometry analysis and the other for trace element analysis. The elements evaluated were vanadium (V), chromium (Cr), copper (Co), nickel (Ni), copper (Cu), zinc (Zn), lead (Pb), rubidium (Rb), strontium (Sr) and zirconium (Zr). Their concentrations were determined using a RIGAKU ZSX Primus II X-ray fluorescence spectrometer system and analysed in pressed powder briquettes. Trace element accuracy was evaluated using the standard CH-1 marine sediment, whose values from each element was: V (111.8%), Cr (98.1%), Co (113.8%), Ni (102.6%), Cu (95.0%), Zn (98.7%), Pb (94.4%), Sr (98.9%) and Zr (97.2%). Texture analysis was determined using a RX-29 Ro-Tap sieve shaker and a standard ASTM sieve from -2, -1, 0, 1, 2, 3 and 4 ϕ. Sediment were classified as mud, sand and gravel based on the methodology proposed by Folk (1980).

A k-means clustering technique was used to group the sampling sites and reveal potential spatial patterns of pollution at Isla del Carmen. K-means is a non-hierarchical, centroid-based partitioning method that maximizes the distances between cluster centroids within each cluster, the centroid represents the point at which the sum of distances of elements in the cluster is the least (Lletí et al., 2004). The optimal number of output clusters was determined using 30 different clustering optimization indices contained within the NbClust (Charrad et al., 2014) package in R. Subsequently, the majority rule was used to select the final number of clusters. Due to the large number of trace elements analysed in this study, a Principal Components Analysis (PCA) based on the correlation matrix with Varimax rotation (Jolliffe, 2002) was used to reduce the dimensionality of the dataset and extract uncorrelated components. Trace elements were used as input variables in the PCA and the resulting component scores were saved as new variables. The number of components to be retained for further analysis was selected based on the Kaiser criterion (eigenvalue >1). The k-means algorithm was conducted using the scores of the selected components as input variables. The analyses were run using the factoextra (Kassambara and Mundt, 2017) and NbClust (Charrad et al., 2014) packages in R.

In addition to the soil parameters and trace elements described above, total rainfall during the rainy season was included to better discern mangrove phenology at study sites. The timing of mangrove phenology events is influenced by environmental factors such as cumulative rainfall, maximum/minimum temperature (Mehling, 2006) maximum/minimum temperature (Mehling, 2006), surface temperature, sea surface temperature and salinity (Songsom et al., 2019). The total rainfall during the rainy season (June to September) was extracted from the Daymet version 4 and computed for the study year (2019). Daymet provides daily gridded estimates of weather parameters for North America, with a 1 km x 1 km spatial resolution (Thornton et al., 2021). Daymet was chosen due its higher spatial resolution, adequate to capture precipitation gradients at Isla del Carmen.

2.3 Remote sensing data collection and processing

In order to model the phenology profiles of mangroves at Isla del Carmen, a multispectral time series was extracted from the Sentinel-2 mission´s products. The Sentinel-2 constellation consists of two satellites (Sentinel-2A and Sentinel-2B) and provides multispectral imagery with a combined revisit time of 5 days and a spatial resolution of 10, 20 and 60 m depending on the specific spectral band. Each Sentinel satellite provides 13 spectral bands. The Sentinel-2 data used in this study was extracted from the Level-2A collection in Google Earth Engine (Gorelick et al., 2017), which corresponds to surface reflectance at each pixel within each Sentinel-2 image. The Level-2A Sentinel data is provided by the European Space Agency (ESA), after applying the sen2cor algorithm for atmospheric correction (Main-Knorn et al., 2017). In total, 60 Sentinel-2 images were used in this study.

Three vegetation indices (VIs) were chosen to characterize mangrove phenology (Table 1). The Red Edge Normalized Difference Vegetation Index (NDVIre) (Gitleson and Merzylak, 1994; Lin et al., 2020) is computed as the normalized difference between the Near Infrared band (wavelength range 785-899 nm and a ground sampling distance of 10 m) and one of the three available Red Edge bands (wavelength range 698-713 nm and a ground sampling distance of 20 m). NDVI versions based on red-edge bands are more sensitive to variations in chlorophyll content than NDVI (Fernández et al., 2016) and have a superior performance in tracking seasonal changes in chlorophyll pigment pool (Lin et al., 2020). Red edge bands have also proven to be highly correlated with wetland vegetation biomass (Naidoo et al., 2019) and leaf chlorophyll content of mangrove forests (Zhen et al., 2021). Specifically, in the context of mangrove vegetation, several publications have demonstrated the higher accuracy of different versions of NDVIre for quantifying mangrove chlorophyll (Heenkenda et al., 2015), high performance in the classification of mangrove species (Behera et al., 2021) and high performance in the estimation of mangrove biomass (Wang et al., 2020). In addition, Pastor-Guzman et al. (2015) suggested that the Sentinel-2 red edge bands should be incorporated in broad band indices in order to increase the accuracy of leaf chlorophyll content estimations in mangroves.

The Green Normalized Difference Vegetation Index (GNDVI) is computed as the normalized difference between the Near Infrared band (wavelength range 785-899 nm and a ground sampling distance of 10 m) and the Green band (wavelength range 543-578 nm and a ground sampling distance of 10 m). Although GNDVI constitutes a broad band-based vegetation index, it has shown very strong correlations with mangrove chlorophyll content from both Landsat-derived (Pastor-Guzman et al., 2015) and in-situ measured reflectance (Gholizadeh et al., 2015).

The Two-band Enhanced Vegetation Index (EVI2) (Jiang et al., 2008) (Table 1) has been extensively used in mangrove vegetation studies (Rahman et al., 2013, Berlanga-Robles and Ruiz-Luna, 2020) due to its ability to overcome limitations associated with the enhanced vegetation index (EVI). Unlike EVI, EVI2 incorporates only the red and near-infrared reflectance, therefore avoiding the atmospheric scattering problems associated to the blue band in EVI (Rahman et al., 2013).

Google Earth Engine was used to extract multispectral information and compute the three VIs between January 2019 and July 2020 in order to visualize the complete mangrove phenological cycle corresponding to the time when the trace element samples were obtained (August 2019). The concentrations of trace elements may show strong seasonal (Olivie-Lauquet et al., 2001) and interannual variability (Li et al., 2021) due to changes in the discharge concentrations and precipitation. Since the main purpose of this study was to relate potential phenology alterations with trace elements and physicochemical elements concentration within the mangrove phenology cycle of 2019-2020, multi-decadal satellite time series and temporal aggregation of satellite images were discarded from the analysis. Both long term time series and multi-temporal aggregation may bring changes in the spectral signature of mangroves due to disturbances and mangrove dynamics that could mask the effect of trace and physicochemical elements. For instance, Younes et al. (2021) point out that long-term mangrove phenology models may also reflect plant migration, colonization and dieback. Sentinel level-2A images were used for the VIs computation for each day of available cloudless imagery. Images with a cloud cover over 20% of the study area were discarded. The QA60 band, containing cloud mask information, was used for this purpose. Band QA60 incorporates information about the location of cirrus and dense clouds at a spatial resolution of 60 m per pixel, which is subsequently resampled at resolutions of 10 and 20 m per pixel.

A 300 m buffer around each study site was generated in order to extract the corresponding mangrove pixels and assess phenology trends in relation to pollutant concentrations. Within each study site, a mangrove mask was created by manually digitizing mangrove areas based on aerial imagery interpretation. The resulting masks were used to extract only mangrove pixels. Manual masking of vegetation has been used in similar phenology studies (Granero-Belinchon et al., 2020). Only pixels with a 100% mangrove coverage were used within each study area subset.

In order to enhance the robustness of the time-series analysis and ensure a coherent comparison between study sites, two filtering criteria were applied to the initial set of study sites. A site was discarded from further analysis if:

1. The share of mangrove coverage was less than 5% of the total study area (300 m buffer around the sampling point).
2. The number of non-contaminated images (absence of clouds, cloud shadows, smoke and faulty pixels) at each study site was greater than 40 for the study period.

2.4 Time series reconstruction

Satellite-derived time series usually contain noisy data due to aerosols, cloud cover or solar-sensor geometry. It is therefore necessary to eliminate noisy or cloudy images, and smooth these datasets using curve-fitting methods. A wide array of curve fitting and smoothing algorithms has been used to approximate satellite-based phenology in mangroves including: Double Logistic and Discrete Fourier Transform (Pastor-Guzman et al., 2018), Generalized Additive Models (Younes et al., 2021), and Harmonic Analysis of Time Series (Li et al., 2019, Valderrama-Landeros et al., 2021). In the absence of validation data, within this study, the VI-based time series at each site were reconstructed using a Harmonic Analysis of Time Series algorithm (HANTS). HANTS algorithm was chosen due to its ability to utilize a time series of irregularly spaced satellite images and the capacity to easily filter out noisy and cloudy observations (Roerink et al., 2000). Additionally, the choice of HANTS was based on the better performance of this technique over other smoothing algorithms. For instance, Julien and Sobrino (2019) demonstrated that within South-East Mexico, HANTS yielded more accurate results than the Iterative Interpolation for Data Reconstruction, Savitzky-Golay, the Asymmetric Gaussian, and the Double Logistic methods. In the context of mangrove phenology, HANTS was found to be less susceptible to the distribution of raw NDVI values than Savitzky-Golay (Wu et al., 2021). Harmonic analysis uses superimposed periodic functions to model signals or functions (Zhou et al., 2015). The HANTS algorithm iteratively fits a least squares curve on the basis of harmonic components, namely sines and cosines (Roerink et al., 2000). During the fitting process, values below the fitting curve are given less weight in the next iteration (Julien and Sobrino, 2019).

HANTS was implemented using the package geoTS (Tecuapetla, 2020) in R (R Core Team, 2020) and the number of harmonics was chosen on the basis of mangrove phenology characteristics and previous research (Julien and Sobrino, 2019). Roerink et al. (2000) stated that there is no objective method to determine the number of harmonics used in a HANTS. In this study, three harmonics were chosen as the optimal number to characterize the phenology at Isla del Carmen. Mangroves in the area of Laguna de Terminos have been previously identified as having a smooth bimodal phenology cycle (Day et al., 1996), similar to other regions of Mexico (Pastor-Guzman et al. 2018). In order to adequately capture this bimodality within one year, three harmonics were chosen instead of two. In addition, Julien and Sobrino (2019) used three harmonics to achieve the most accurate HANTS reconstructions in evergreen vegetation regions characterized by low seasonal amplitude. Finally, it has been suggested that higher order harmonics can introduce noise in the phenology approximations, ultimately lowering the ability of HANTS to detect outliers (Zhou et al., 2015).

2.5 Comparison between vegetation indices

Assessing and comparing the ability of different vegetation indices to extract phenology metrics requires validation data obtained from in-situ observations. However, within this study, in-situ validation data was not collected due to the lack of an adequate phenological observation network. In the absence of ground truth data, the fitting performance of NDVIre, GNDVI, and EVI2 was examined. The HANTS reconstructed time series were assessed against the raw values of each VI at each study site using the coefficient of determination (R^2). The R^2 between reconstructed time series and raw VI values represent a measure of VI suitability and sensitivity to noise. A one-way ANOVA with post-hoc Tukey HSD test was used to examine whether statistically significant differences ($p < 0.05$) existed between the R^2 values among the three VIs. The VI that showed the highest R^2 between fitted and raw values was chosen for further phenology analysis.

2.6 Phenology assessment

Mangroves in Isla del Carmen show a distinct phenological pattern, reflected in the values of VIs throughout the season, with the lowest values between May and July, and the highest values between January and February (Figure 2). However, the exact timing of greenup, senescence and mangrove growth peak may vary considerably across sites. In order to characterize mangrove phenology changes in relation to pollution and physicochemical and geochemical characteristics, a number of metrics were extracted from the HANTS-derived phenology profiles at each study site. The phenology metrics are listed and described in Table 2 and illustrated in Figure 3.

Several methods have been proposed to extract phenology metrics from satellite-based times series (Bórnez et al., 2020; Shang et al., 2017) such as percentile thresholds (Verger et al., 2016), first derivative (Tateishi and Ebata, 2014), or inflection-based methods (Zhang et al., 2003). In order to avoid the subjectivity associated with percentage threshold methods, an inflection approach based on the maximum change ratio was utilized. The maximum change ratio (Jeong et al., 2011) detects the point within the VI trend when the increasing or decreasing trend reach a maximum or a minimum, and is formulated as follows:

$$VI_{ratio(t)} = \frac{\left[VI_{(t+1)} - VI_{(t)}\right]}{VI_{(t)}} \quad (1)$$

Where

$VI_{ratio(t)}$: Change ratio of the vegetation index at time *t*.

$VI_{(t)}$: Value of the vegetation index at time *t*.

$VI_{(t+1)}$: Value of the vegetation index at time *t+1*.

Start of Season (SoS) was determined as the day when the increasing VI rate reaches the maximum, whereas the End of the Season (EoS) corresponds to the date when the decreasing VI trend reaches the minimum. Length of Season (LoS) was subsequently calculated as the difference in days between EoS and SoS. Peak of Season (PoS) was determined as the day of the year when VI reaches its maximum value and seasonal amplitude was defined as the difference between the maximum and minimum values of VI for that particular season. All the phenology metrics described above were derived from the HANTS phenology profiles calculated at each sampling point.

2.7 Relationships between environmental variables, pollutant concentration and phenology metrics

Responses of vegetation phenology to pollution are likely to be non-linear. In order to avoid an oversimplified characterization of the relationships between mangrove phenology and pollution in

Isla del Carmen, Generalized Additive Models (GAMs) were utilized. GAMs are defined as semi-parametric extensions of Generalized Linear Models (GLMs), with the ability to resolve non-linear relationships (Guisan et al., 2002). GAMs have gained popularity in ecology, among other fields, due to their capacity to estimate complex non-linear relationships by replacing the parametric terms of a GLM by smooth functions of the covariates (Simpson, 2018). A GAM can be represented as:

$$y = \beta_0 + \sum_{j=1}^{p} s_j(x_j) \tag{2}$$

Where

y: Response variable

B_0: Intercept

$S_j(x_j)$: Vector of smoothing functions of the predictor variables

The analysis was set as a two-step process: Variable selection and modelling and visualization.

2.7.1. Variable selection for GAMs

Variable selection is a necessary step in GAMs with multiple covariates, in order to unveil the covariates that have the strongest effect on the response variable, as well as improving model prediction accuracy (Marra and Wood, 2011). Several variable selection procedures have been proposed, including the double penalty approach, in which the first penalty component controls the wiggliness of the fitted trend in the smooth terms (Simpson, 2018), whereas the extra penalty component penalizes functions in the null space (Marra and Wood, 2011). Other authors have used backward stepwise selection methods (Marra and Wood, 2011), fitting all covariates simultaneously and subsequently excluding covariates and re-assessing model robustness. However, within this study, the large set of covariates and the relatively small set of samples limits the number of covariates that can be simultaneously fitted in a GAM, therefore hindering the use of these selection techniques (Marra and Wood, 2011).

In order to overcome these limitations, a two-step method was used:

Step 1 – Single variable GAMs. A GAM model was constructed for each phenology response variable (SoS, PoS, LoS, seasonal amplitude and growth peak) and each covariate (geochemical variables, trace elements and climatic variables). GAMs were fitted in R using the mgcv package (Wood, 2017). The restricted maximum likelihood (REML) was chosen as the smoothing parameter estimation method. In addition, a thin plate spline was fit as the smoothing term of each covariate. Simpson (2018) recommends REML as the best method to fit GAMs when dealing with models with one single covariate. The alternative generalized cross-validation (GCV) method tends to undersmooth, producing overly wiggly splines (Simpson, 2018).

Step 2 – Covariate pre-selection. The pre-selection of variables was undertaken on the basis of the explained deviance and the approximate significance of the effect of the smooth terms on the response variable. The percentage of deviance explained is similar to the coefficient of determination in regression models and represents the likelihood of significant effects of covariate in the response variable. Covariates with a percentage of deviance explained over 10% and a $p < 0.01$ were selected for further analysis.

2.7.2. Model optimization and visualization

For each of the phenology response variables, a GAM was re-fitted incorporating only the covariates selected in the first step, following a forward stepwise selection procedure. At each step, an explanatory variable was added to the model following a ranked order of deviance explained. After each individual covariate was added to the model, the percentage of deviance explained by the overall model was re-calculated, as well as the Aikake's Information Criterion (AIC). The covariate was then retained if it would decrease the model's AIC and maintain or increase the model's explained deviance. This model optimization process was undertaken using the *mgcv* package in R (Wood and Wood, 2015). In order to characterise phenology responses, each pair of phenology response variables and covariates was visualized individually within each model. Plots were constructed using *ggplot2* package in R (Wickham, 2011).

3. Results

3.1. Spatial clustering of study sites

Following the Kaiser criterion, three components were retained in the PCA, accounting for 89.9 % of total variance explained. Table 3 presents the results of the PCA, including the percentage of variance, cumulative percentage of variance and the component loadings. The first component explained 41 % of the variance and was strongly correlated with V, Co, Ni and Rb. The second and third components explained 30.4 % and 18.4 % of the variance and were strongly correlated with Cu, Zn, Pb and Cr, Ba and Zr respectively.

Following the PCA, a K-means clustering analysis was undertaken. The assessment for optimal number of clusters based on multiple indices revealed that, according to the majority rule, the best number of clusters was 4, including 13, 12, 10 and 1 study sites in each cluster respectively. The spatial configuration of the clustered study sites is shown in figure 4, indicating a relatively mixed pattern of study site clusters. Cluster 1 is mainly located in the central section of Isla del Carmen, which is mostly dominated by mangroves. However, clusters 2 and 3 are both associated to the urban area as well as the North East section of the island. Cluster 4 includes only study site nr 6 due to the exceptionally high level of trace elements recorded at the site.

In order to better understand the results of the K-means clustering, boxplots for the mean concentrations of each trace element within each cluster were calculated (see Appendix A, figure S1). Cluster 4 was excluded from this analysis in order to allow for better comparisons among clusters. Cluster 1 shows lower median values for the concentrations of most trace elements. However, higher values of Sr can be observed in Cluster 1 compared with Cluster 3. Cluster 3 is characterized by higher concentrations of most trace elements under analysis. In Cluster2, elevated concentrations of Cr, Sr, Ba and Zr can be observed.

3.2. Suitability of vegetation indices and phenology assessment

Phenology profiles were calculated for 29 study sites using three different VIs (NDVIre, GNDVI and EVI2). The HANTS phenology curves showed clear differences in the fitting performance among the three VIs (Table 4). ANOVA and Tukey tests showed that the fitting accuracy of NDVIre was significantly higher than that of GNDVI and EVI2 ($p < 0.0001$), with average R^2 values across study sites of 0.503, 0.356 and 0.357 respectively. This reveals a more pronounced scattering of the GNDVI and EVI2 values around the smoothed phenology curves. Due to its higher fitting performance, NDVIre was selected for further analysis.

Figure 5 shows the NDVIre-based phenology profiles at three study sites along Isla del Carmen, modelled using a HANTS algorithm. These sites have been chosen to illustrate a gradually increasing degree of pollution throughout the 3 main clusters. The temporal evolution of NDVIre through the season shows distinct patterns at the three sites. Site 8 corresponds to the mangroves in Laguna Caracol, located within the Southern coast of Ciudad del Carmen (Figure 1) and it is subjected to frequent wastewater discharge. This site shows a lower peak of greenness compared to sites 16 and 32, as well as a delayed timing of the growth peak and start of the season. NDVIre at Site 8 also shows a slightly smaller seasonal amplitude compared with Sites 16 and 32. Although sites 32 and 16 are characterized by a similar degree of vegetation vigour, the greenup period shows considerable differences between both locations. Site 16, located within cluster 2, is subject to a delayed start of the season, alongside a delayed timing of the growth peak. Site 16 is located towards the eastern edge of Ciudad del Carmen, while site 32 is situated in the easternmost coast of Isla del Carmen, within cluster 1 and distant from urban pollution sources.

3.3. Relationships between environmental variables, pollutant concentration and phenology metrics

3.3.1 Variable selection

The two-step variable selection procedure highlighted the physicochemical, textural parameters and pollutants that have the strongest effect on the phenology response variables using single-variable GAMs (Table 5). Start of season (SoS) and length of the season (LoS) showed a significant response to the largest set of covariates, including concentrations of Pb, Cu and Zn, as well as salinity, and pH. Peak of season (PoS) was also affected by a wide set of covariates including salinity, pH, % of silt, and concentrations of Cu. It is worth noting that Cu and Pb strongly affect both the SoS and the LoS. More precisely, Cu explained 56.9% and 56% of the deviance in SoS and LoS respectively, whereas Pb explained 49.3% and 44.3% of the deviance in SoS and LoS. Similarly, salinity alone conveys an explanatory rate of 43.9% on the SoS and 40.2% on the peak of season (PoS), indicating the strong dependence of these phenology metrics on salinity. Growth peak, which is likely to be related to overall mangrove health and productivity, showed a strong significant response to Sr, with a 33.9% of deviance explained. Seasonal amplitude showed no significant response to any of the covariates.

3.3.2 Model optimization

GAMs were optimized following a forward stepwise selection procedure. Table 6 includes the covariates used in each of the four GAMs, alongside with the percentage of deviance explained by each model and the adjusted R-squared.

The highest explanatory rate was achieved by Model 1 (92.1%, $R^2 = 0.88$), showing that the SoS in mangroves in Isla del Carmen is strongly influenced by concentrations of Cu and Pb, and physicochemical parameters (salinity and pH). Model 2 showed a very similar trend on the LoS whereas model 4 showed the influence of Sr on the growth peak. Specifically, Sr explained a large amount of deviance in growth peak, suggesting a strong influence of this trace element on the vigour of mangroves. After the model optimization process, Model 3 retained only physicochemical variables (Salinity, pH and % silt) to assess the response of PoS, with 43.6 % of deviance explained.

Further analysis was undertaken to explore the nature and shape of altered phenology patterns in relation to trace elements and physicochemical parameters variables. GAMs plots show that these relationships are in many cases non-linear. For instance, figure 6 shows different responses of SoS concentrations of Pb and Cu led to a delayed start of the greenup period (represented as accumulated Day of the Year [DOY]) following a nonlinear trend, where the increasing trend was sharpest at lower concentrations of Pb and gradually decreased as the concentration of trace elements increased. Increased pH led to an almost linear increase in the Start of the Season, indicating an increasingly delayed start of the greenup period as pH increases. Conversely, increased salinity led to an earlier SoS.

Figure 7 shows the curves fitted to the LoS and concentrations of Cu and Zn, as well pH and salinity, corresponding to the single-variable GAMs (Model 2). LoS is shortened as a response to both Cu and Zn increased concentrations, following non-linear trend. increased pH also leads to a shortening of the season, whereas increased salinity expands the growing season length.

Figure 8 shows changes in PoS date (represented by the DOY during the season under assessment within this study, corresponding to Model 3), as well as changes in the growth peak (model 4). As shown in Table 5, PoS is strongly influenced by salinity. As salinity decreases, the peak of greenness occurs later in the season, following an almost linear relationship. On the other hand, increased pH led to a delay in the PoS, steadily more pronounced as pH increases. The percentage of silt in the sediment also influences the PoS date, although this relationship is more subtle. PoS slightly decreases as the percentage of silts increases, but this trend shifts slowly as the % silt in the sediment continues to increase. Growth peak shows a slight increase as Sr concentrations increase, although this relationship shifts gradually towards a sharp decrease with increased concentrations of Sr.

4. Discussion

The results from this study clearly show an impact of trace elements and environmental variables on the phenology of mangroves in Isla del Carmen. Altered phenology in mangroves has been shown to be linked to changes in biomass and forest structure (Agraz Hernandez et al. 2011; Robertson et al. 2020), which in turn has been shown to influence ecosystem service provision particularly carbon and environmental contaminant sequestration and storage (Kathiresan et al. 2013; Numbere & Camilo 2018; Sasmito et al. 2019; Simpson et al. 2019).

4.1 Clustering of study sites and potential sources of pollution.

The cluster analysis (Figures 4 and S1) highlighted that the north coast forms a characteristic area where mangroves are subject to higher levels of Cr, Sr, Ba, and Zr (Cluster 2). In addition, most study sites grouped in cluster 3 are located within Ciudad del Carmen, indicating that Pb pollution sources are predominantly from urban runoff. Cluster 4 is a single-site cluster located at a sewage and wastewater discharge point, and characterized by exceptionally high levels of pollution. Sites within cluster 1 are characterized by relatively lower concentrations of trace elements, and are predominantly located in pristine areas of the island. These results were similar to those reported by Celis et al. (2020). The authors noted that although mineralogy and sediment texture were natural drivers that control trace element distribution in mangroves from Isla del Carmen, at least Pb, Zn, and Cu were derived from point sources such as city sewage and boat yards, elements such as V, Ni, and Cr were linked to the presence of mafic rocks, while Ba and Zr were likely to be related and oil industry origin, although there was not enough evidence to conclusively support this.

4.2 Phenological changes using remote sensing tools.

Phenology in mangroves is influenced by a range of seasonably varying factors including precipitation, temperature, humidity, day-length (Kamruzzaman et al., 2012; Lima et al., 2012; Torres et al. 2018; Peel et al., 2019), or large-scale impacts such as storm surges, alterations to hydrology, or erosion (Zhang et al., 2016; Small and Sousa, 2019). As such there can be substantial regional variations in mangrove phenology as noted by Songsom et al. (2019) for Thailand. Mangrove phenology can also be impacted by environmental stressors such as trace elements and organic pollutants, which can vary over much smaller scales, particularly where point source pollution is the cause (Rani et al., 2016).

The accumulation of trace elements in mangroves can affect the functioning of these ecosystems. A range of studies have shown that where trace element contamination occurs in mangrove sediments, this is taken up in the roots of mangroves and transported to other tissues in the plant (Mandura, 1997; Agoramoorthy et al., 2008; Lewis et al., 2011; Bayen, 2012; Maiti and Chowdhury, 2013; Arrivabene et al., 2015). The highest concentrations are typically found in the roots with lower concentrations in the leaves (Arrivabene et al. 2015), although differing trace elements have different levels of mobility in the plant tissues (Maiti and Chowdhury, 2013). Agoramoorthy et al. (2008) have shown that trace elements in mangrove trees and associate understory halophytes, can reduce plant productivity. Disturbances have also been shown to delay the onset of greater productivity during the phenological cycle (Zhang et al., 2016).

Remote sensing has been noted as an appropriate tool to estimate mangrove apparent phenology, showing a high degree of agreement with in-situ plant phenology observations (Pastor-Guzman et al., 2018). In particular, recent developments in cloud computing software such as Google Earth Engine have substantially improved the assessment of the state of vegetation status and phenology, including mangrove vegetation (Li et al., 2019). Satellite-derived vegetation indices are a key element in most studies related to remotely sensed phenology. However, sensitivity to environmental conditions and local biophysical characteristics across different vegetation indices is highly variable. Consequently, the choice of spectral index has an impact on the extraction of phenology dates and the detection of phenological changes. In this study, NDVIre showed the highest degree of agreement between original and predicted values along the phenology profiles, indicating a much lower amount of scattering and noise than EVI2 and GNDVI. This is likely because EVI2 and EVI were specifically designed for MODIS (Huete et al., 2002) and may bear inaccuracies when derived from Sentinel-2 or Landsat sensors. On the other hand, GNDVI is a broadband spectral index, which although sensitive to chlorophyll concentrations, may still show a limited ability to detect subtle structural changes in canopies. Valderrama-Landeros et al. (2021) suggested that the Sentinel red-edge band may improve phenology assessments in mangroves. The present study confirms the benefits of using red edge bands in phenology assessments. The narrower spectral range of the red edge band (698-713 nm) leads to lower scattering of values of NDVIre along the reconstructed phenology profile and consequently a better fitting performance.

In the present study, a Harmonic Analysis of Time Series (HANTS) was utilized to estimate phenology trends and detect potential phenology shifts over the mangroves in Isla del Carmen, Mexico. HANTS has been previously shown to provide a robust approximation of phenology from remotely sensed data sources (Julien and Sobrino, 2019). The results of this study indicate that the presence of trace elements may trigger shifts in the phenology of mangroves in the study area. A delay in start of season (SoS) and a shortening of the season linked to Pb, Cu, and Zn was observed for mangroves that are adjacent to the city of Carmen. The gradually decreasing trend between SoS and Pb and Cu suggests that under certain heavy metal concertation levels, mangroves no longer show delays in the timing of the SoS. Trace element pollution from urban sources, alongside pH and salinity, explain a large share of the deviance in the SoS and the length of the season (LoS). Celis et al., (2020) used pollution indices applied in sediments to suggest that high concentrations of Pb, Zn, and Cu reported in the urban mangroves of Isla del Carmen would likely impact mangrove vegetation as well as associate organisms. The pollution indices used by Celis et al. (2020) highlighted that sites impacted by point source pollution exhibited severe enrichment and very severe enrichment, and were classified as heavily polluted and extremely polluted mangrove environments by these trace elements. The mangrove phenology analysis undertaken in this study showed the pollution impacts on mangrove vegetation caused by trace elements.

The growth peak showed responses to Sr. Notably, Sr explained 33.9% of the deviance of growth peak within the single-variable Generalized Additive Model. The visualization of this specific model indicated an overall decrease of the growth peak associated to increased concentrations of Sr. This relationship suggests an overall decrease in mangrove vigour Sr increases. Sr is a common environmental trace element, that is readily absorbed by plants due to its similarity to Ca an essential element for plant growth (Burger and Lichtscheidl, 2019). Stable isotopes of Sr can have a detrimental impact on plant growth replacement of Ca during uptake, resulting in Ca deficiency (Burger and Lichtscheidl, 2019). Sr uptake in trees is influenced by root morphology, soil type, pH, and climate (Mcculley et al., 2004, Poszwa et al., 2004 and Reynolds et al., 2012), although there have been few studies investigating the ecotoxicological impact on mangrove plants (Kulkarni et al. 2018). In coastal and estuarine environments, rock weathering, rain, and marine aerosols have been identify as natural sources of Sr, while fertilizers used in agriculture and barite used in oil drilling have been identified as anthropogenic sources (Torres et al 2002, Zielinsky et al. 2018, Fang et al 2018, Elkatatny, 2019). In the mangroves of Isla del Carmen, Celis et al. (2020) have shown that while the bulk of the Sr appears to be derived from natural sources, there is some moderate anthropogenic enrichment.

The Generalized Additive Models utilized in this study also show phenology responses to pH and salinity, in accordance to the results obtained in the Yucatán peninsula by Pastor-Guzmán et al. (2018) and more recently Chamberlain et al. (2021) for Australia. The negative correlations between the peak of season (PoS) and salinity suggest an earlier timing for the growth peak as salinity increases. On the other hand, increased pH led to a delayed PoS and SoS. These results suggest that the phenological alterations are caused by physicochemical parameters in mangroves from Isla del Carmen. Although mangroves are organisms adapted to high salt concentrations, Xu et al., (2014) reported that mangrove biomass was inversely related to salinity meaning that salt decreased the photosynthetic rate of mangroves. Very high salinity also inhibits growth and nutrient assimilation in these plants (Bannerjee et al., 2017; Shiaou et al., 2017) and can change the community ecology. Alterations in salinity can also alter the bioavailability of some trace element contaminants (Lacerda et al., 2021). pH has an indirect relationship to mangroves phenology, because usually pH can influence nutrient adsorption, which can lead to phenological changes in mangroves. For example, Neina et al. (2019) reported that nutrients were less available for mangrove plants with lower soil acid conditions due to low adsorption and high desorption rates.

This study demonstrates that the impacts of point source pollution in mangroves may result in subtle changes in phenology. Although these altered phenological patterns could strongly affect the capacity of mangroves to deliver key ecosystem services, the nature and spatial characteristics of these changes hinder their detection and quantification. In this regard, time-series derived from satellite data constitute an effective tool to unveil phenology shifts and alterations.

4.3 Limitations and sources of uncertainty

Despite the vast potential of Sentinel imagery for mangrove phenology assessments, some constraints should be considered within this study. As pointed out by Younes et al. (2020), phenology assessments based on remotely sensed data are an approximation of the real phenology of vegetation and as such, a certain degree of uncertainty is involved. The choice of vegetation indices as well as smoothing algorithms has an impact on the extraction of phenology metrics from remotely sensed data and consequently, results may be highly variable. In this regard, there is no "one size fits all" index or algorithm and each case should be evaluated separately. The role of ground truth data to discern the most accurate satellite-based phenology reconstruction techniques is crucial (Nagai et al., 2020). Within this study, the absence of validation data constituted an important source of uncertainty, as it impeded comparisons between vegetation indices and smoothing algorithms. In order to compensate for this, the choice of NDVIre was based on a R-squared goodness-of-fit assessment. The choice of HANTS was based on recently published data that indicates the good performance of the algorithm both in the context of mangrove ecosystems and the location of the area under study. Future phenology studies in Isla del Carmen should aim at collecting a comprehensive set of in situ validation data and coupling it with satellite-based data. A study by Pastor-Guzman et al. (2018) focused on the phenology of mangroves using MODIS imagery along the coast of Yucatán peninsula in the nearby states of Yucatán and Quitana-Roo. The SoS modelled by the Pastor-Guzman et al. (2018) study occurred at DOY 184, 200 and 220 measured by EVI, NDVI and gNDVI respectively. The present study revealed very similar dates, with an average timing of SoS on DOY 223. Moreover, both studies show similarities in the timing of the growth peak. Pastor-Guzmán reported growth peak at DOY 332, 348 and 360 for EVI, NDVI and gNDVI respectively and an earliest and latest DOY of 280 and 40 detected by EVI. The present study revealed an average DOY of 29 across the study sites detected by NDVIre. These comparisons do not substitute a validation assessment, but show that the combination of NDVIre and HANTS yields results consistent with the phenology trends in the region.

Another source of uncertainty within in this assessment was the description of a single-year phenology cycle. This decision was driven by the need to relate phenology patterns with the concentrations of trace elements and physicochemical parameters in 2019. Ideally, data on trace elements and physicochemical parameters would have been collected throughout several years and consequently related to multiple phenology cycles, therefore yielding a more complete overview of mangrove phenology responses at Isla del Carmen. However, long term mangrove phenology models could also reveal patterns of phenology change associated to mangrove vegetation dynamics, natural disturbances and climate change. In order to better focus on the effect of trace elements and physicochemical parameters in 2019, only one phenology cycle was addressed.

4.4 Implications for management

Phenology change detection in mangroves is important to assess broader ecosystem changes and for restoration planning (Upadhyay and Mishra, 2010). Alterations to phenology can have an influence on the productivity of mangroves as well as alter detrital deposition, which can have knock-on effects on carbon storage and the detrital food chain, highly valuable ecosystem services (Duke 1988, Wafar, 1997, Songsom 2019). While the mangroves in this current study are not shown to be highly degraded, trace elements have been shown to influence phenological characteristics, which is likely to be a precursor to ecosystem degradation should contamination levels increase. The evaluation of impacts on phenology in mangroves using remotely sensed data, could therefore be used as an early warning system for management intervention to initiate close monitoring to prevent large scale ecosystem degradation and potential associated loss of ecosystem service provision within the mangroves.

5. Conclusions

The results of this study revealed spatial patterns of trace elements contamination in mangroves at Isla del Carmen. Mangroves situated in urban environments as well as those located in the North East section of the island are contaminated by most trace elements under study (e.g. Pb and Cu). Clusters 2 and 3 presented the highest pollution levels and show distinct patterns, with Cluster 2 encompassing the highest levels of Cr, Sr, Ba, and Zr and Cluster 3 the highest levels of V, Co, Ni, Cu, Zn, Pb, and Rb. HANTS smoothing algorithms in combination with GAMs were used to further extract phenology parameters and detect phenology shifts in relation to environmental variables and trace elements. The results suggest that the dominant mangrove flora at the study sites show a phenological response to physicochemical parameters in seawater and trace element concentrations in sediment. Among the various phenology shifts in mangroves at Isla del Carmen, the timing of the Start of the Season showed a linear delay in response to pH and a non-linear delay in response to Pb and Cu. The timing of the Peak of Season showed significant responses only to physicochemical parameters, while the growth peak decreased in response to increased Sr concentrations. The effect of trace element contamination and physicochemical parameters on the onset of the growth season and the growth peak in mangroves likely has an impact on the functioning of mangrove ecosystems, including a decrease in the ability to resist extreme weather events and reduced carbon storage and sequestration through decreases in autochthonous inputs

This study also acknowledges the need to utilize ground truth data in order to select the most adequate vegetation indices and smoothing algorithms, as well as avoid potential uncertainties arising from the use of remote sensing data. It is also suggested to undertake a long-term monitoring scheme of trace elements in mangroves at Isla del Carmen and assess the effects of pollution on multi-annual mangrove phenology.

References

Agoramoorthy, A., Chen, F., Hsu, M. (2008). Threat of heavy metal pollution in halophytic and mangrove plants of Tamil Nadu, India. Environmental Pollution. 155(2), 320-326. doi: 10.1016/j.envpol.2007.11.011

Arrivabene, H., Da Costa Souza, I., Oliveira Có, W., Moreira Conti, M., Wunderlin, D., Dias Milanez, C. (2015). Effect of pollution by particulate iron on the morphoanatomy, histochemistry, and bioaccumulation of three mangrove plant species in Brazil. Chemosphere. 127, 27-34. doi: 10.1016/j.chemosphere.2015.01.011

Balogun, A., Yekeen, S. T., Pradhan, B., & Althuwaynee, O. F. (2020). Spatio-Temporal Analysis of Oil Spill Impact and Recovery Pattern of Coastal Vegetation and Wetland Using Multispectral Satellite Landsat 8-OLI Imagery and Machine Learning Models. Remote Sensing, 12(7), 1225. doi:10.3390/rs12071225

Banerjee, K., Gatti, R.C. and Mitra, A. (2017). Climate change-induced salinity variation impacts on a stenoecious mangrove species in the Indian Sundarbans. Ambio, 46(4), pp.492-499. doi: 10.1007/s13280-016-0839-9

Barnes, B.B., Hu, C., Kovack, C., Silverstain, R.N. (2015). Sediment plumes induced by the Port of Miami dredging: Analysis and interpretation using Landsat and MODIS data. Remote Sensing of Environment. 170, 328-339. doi: 10.1016/j.rse.2015.09.023

Bayen, S. (2012). Occurrence, bioavailability and toxic effects of trace metals and organic contaminants in mangrove ecosystems: A review. Environment International, 48, 84-101. doi: 10.1016/j.envint.2012.07.008

Behera, M. D., Barnwal, S., Paramanik, S., Das, P., Bhattyacharya, B. K., Jagadish, B., . . . Behera, S. K. (2021). Species-Level Classification and Mapping of a Mangrove Forest Using Random Forest—Utilisation of AVIRIS-NG and Sentinel Data. Remote Sensing, 13(11), 2027. doi:10.3390/rs13112027

Berlanga-Robles, C. A., & Ruiz-Luna, A. (2020). Assessing seasonal and long-term mangrove canopy variations in Sinaloa, northwest Mexico, based on time series of enhanced vegetation index (EVI) data. Wetlands Ecology and Management, 28(2), 229-249. doi: 10.1007/s11273-020-09709-0

Blondeau, D., Gower, J.F.R., Dekker, A.G., Phinn, S.R., Brando, V.E. (2014). A review of ocean color remote sensing methods and statistical techniques for the detection, mapping and analysis of phytoplankton blooms in coastal and open oceans. Progress in Oceanography. 123, 123-144. doi: 10.1016/j.pocean.2013.12.008

Bórnez, K., Descals, A., Verger, A., Peñuelas, J. (2020). Land surface phenology from VEGETATION and PROBA-V data. Assessment over deciduous forests. International Journal of Applied Earth Observation and Geoinformation. 84, 101974. doi: 10.1016/j.jag.2019.101974

Burger,A. and Lichtscheidl, I. (2019). Strontium in the environment: Review about reactions of plants towards stable and radioactive strontium isotopes. Science of The Total Environment, 653, 1458-1512. doi: 10.1016/j.scitotenv.2018.10.312.

Canales, J.C., Pérez, R., Zaldivar, M.A., Merino, M., Cardoza, G., Cardoso, J,G. (2019). The effect of mangrove restoration on avian assemblages of coastal lagoon in southern Mexico. PeerJ. 7:e7493. doi: 10.7717/peerj.7493

Capdeville, C., Abdallah, K., Buffan-Dubau, E., Lin, C., Azemar, F., Lambs, L., Fromard, F., Rols, J.L., Leflaive, J. (2018). Limited impact of several years of pretreated wastewater discharge on fauna and vegetation in a mangrove ecosystem. Marine Pollution Bulletin. 129, 379-391. doi: 10.1016/j.marpolbul.2018.02.035

Carvalho, F.P., Villeneuve, J.P., Cattini, C., Rendon, J., Mota de Oliveira, J. (2009). Pesticide and PCB residues in the aquatic ecosystems of Laguna de Terminos, a protected area of the coast of Campeche, Mexico. Chemosphere. 74, 988-995. doi: 10.1016/j.chemosphere.2008.09.092

Celis, O., Giron, P.M., Ontiveros, J., Canales, J., Pérez, R., Ward, R.D., Acevedo, O., Merino, M. (2020). Environmental risk of heavy metals in mangrove ecosystems: An assessment of natural vs oil and urban inputs. Science of the Total Environment. 730, 138643. doi: 10.1016/j.scitotenv.2020.138643

Chamberlain, D. A., Phinn, S. R., & Possingham, H. P. (2021). Mangrove Forest Cover and Phenology with Landsat Dense Time Series in Central Queensland, Australia. Remote Sensing, 13(15), 3032. doi:10.3390/rs13153032

Charrad, M., Ghazzali, N., Boiteau, V., & Niknafs, A. (2014). NbClust: an R package for determining the relevant number of clusters in a data set. Journal of statistical software, 61(1), 1-36.

Connolly, R., Connolly, F., Hayes, M. (2020). Oil spill from the Era: Mangroves taking eons to recover. Marine Pollution Bulletin. 153, 110965. doi: 10.1016/j.marpolbul.2020.110965

CONABIO, (2013).'Mapa de uso del suelo y vegetación de la zona costera asociada a losmanglares, Region Península de Yucatán (2010).', escala: 1:50000. edición: 1.Comisión Nacional para el Conocimiento y Uso de la Biodiversidad. Proyecto: GQ004,Los manglares de México: Estado actual y establecimiento de un programa de mon-itoreo a largo plazo: 2da y 3era etapas. México, DF

Cârlan, I., Mihai, B., Nistor, C., & Große-Stoltenberg, A. (2020). Identifying urban vegetation stress factors based on open access remote sensing imagery and field observations. Ecological Informatics, 55, 101032. doi:10.1016/j.ecoinf.2019.101032

Day, J., Coronado-Molina, C., Vera-Herrera, F., Twilley, R., Rivera-Monroy, V., Alvarez-Guillen, H., . . . Conner, W. (1996). A 7 year record of above-ground net primary production in a southeastern Mexican mangrove forest. Aquatic Botany, 55(1), 39-60. doi:10.1016/0304-3770(96)01063-7

De Lima Nadia, T., Morellato, L. P., & Machado, I. C. (2012). Reproductive phenology of a northeast Brazilian mangrove community: Environmental and biotic constraints. Flora - Morphology, Distribution, Functional Ecology of Plants, 207(9), 682-692. doi:10.1016/j.flora.2012.06.020

Duke, N. C. (1988). Phenologies and litter fall of two mangrove trees, Sonneratia alba Sm. and S. caseolaris (L.) Engl., and their putative hybrid, S.× gulngai NC Duke. Australian Journal of Botany, 36(4), 473-482. doi: 10.1071/BT9880473

Elkatatny, S. (2019). Mitigation of barite sagging during the drilling of high-pressure high-temperature wells using an invert emulsion drilling fluid. Powder Technology. 352, 325-330. doi: 10.1016/j.powtec.2019.04.037

Fang, J.K.H., Rooks, C.A., Krogness, C.M., Kutti, T., Hoffmann, F., Bannister, R.J., (2018). Impact of particulate sediment, bentonite and barite (oil-drilling waste) on net fluxes of oxygen and nitrogen in Artic-boreal sponges. Environmental Pollution. 238, 948-958. doi: 10.1016/j.envpol.2017.11.092

Fernández, A., Fernández, O., Quintano, C. (2016). SENTINEL-2A red-edge spectral indices suitability for discriminating burn severity. International journal of applied earth observation and geoinformation. 50, 170-175. doi: 10.1016/j.jag.2016.03.005

Folk, R.L. (1980). Petrology of Sedimentary Rocks. Hemphill Publications, Austin Texas, p. 182.

Garonna, I., de Jong, R., & Schaepman, M. E. (2016). Variability and evolution of global land surface phenology over the past three decades (1982–2012). Global Change Biology, 22(4), 1456-1468. doi: 10.1111/gcb.13168

Gholizadeh, H., Robeson, S. M., & Rahman, A. F. (2015). Comparing the performance of multispectral vegetation indices and machine-learning algorithms for remote estimation of chlorophyll content: a case study in the Sundarbans mangrove forest. International Journal of Remote Sensing, 36(12), 3114-3133. doi: 10.1080/01431161.2015.1054959

Giri, C., Long, J., & Tieszen, L. (2011). Mapping and Monitoring Louisianas Mangroves in the Aftermath of the 2010 Gulf of Mexico Oil Spill. Journal of Coastal Research, 277, 1059-1064. doi:10.2112/jcoastres-d-11-00028.1

Gitelson, A. A., Kaufman, Y. J., & Merzlyak, M. N. (1996). Use of a green channel in remote sensing of global vegetation from EOS-MODIS. Remote sensing of Environment, 58(3), 289-298. doi: 10.1016/S0034-4257(96)00072-7

Gitelson, A., & Merzlyak, M. N. (1994). Spectral Reflectance Changes Associated with Autumn Senescence of Aesculus hippocastanum L. and Acer platanoides L. Leaves. Spectral Features and

Relation to Chlorophyll Estimation. Journal of Plant Physiology, 143(3), 286-292. doi:10.1016/s0176-1617(11)81633-0

Gorelick, N., Hancher, M., Dixon, M., Ilyushchenko, S., Thau, D., Moore, R. (2017). Google Earth Engine: Planetary-scale geospatial analysis for everyone. Remote sensing of Environment. 202, 18-27. doi: 10.1016/j.rse.2017.06.031

Granero-Belinchon, C., Adeline, K., Lemonsu, A., & Briottet, X. (2020). Phenological dynamics characterization of alignment trees with sentinel-2 imagery: A vegetation indices time series reconstruction methodology adapted to Urban areas. Remote Sensing, 12(4), 639. doi: 10.3390/rs12040639

Guisan, A., Edwards Jr, T. C., Hastie, T. (2002). Generalized linear and generalized additive models in studies of species distributions: setting the scene. Ecological modelling. 157(2-3), 89-100. doi: 10.1016/S0304-3800(02)00204-1

Heenkenda, M. K., Joyce, K. E., Maier, S. W., & Bruin, S. D. (2015). Quantifying mangrove chlorophyll from high spatial resolution imagery. ISPRS Journal of Photogrammetry and Remote Sensing, 108, 234-244. doi: 10.1016/j.isprsjprs.2015.08.003

Huete, A., Didan, K., Miura, T., Rodriguez, E. P., Gao, X., & Ferreira, L. G. (2002). Overview of the radiometric and biophysical performance of the MODIS vegetation indices. Remote sensing of environment, 83(1-2), 195-213. doi: 10.1016/S0034-4257(02)00096-2

Huxham, M., Dencer, A., Diele, K., Kathiresan, K., Nagelkerken, I., Wanjiru, C. (2017). Mangroves and People: Local Ecosystem Services in a Changing Climate. Mangrove Ecosystems: A Global Biogeographic Perspective, 245-274.

INEGI (2018). Anuario Estadistico del Estado de Campeche. Instituto Nacional de Estadistica, Geografía e Informática (In Spanish).

Jeong, S. J., HO, C. H., GIM, H. J., & Brown, M. E. (2011). Phenology shifts at start vs. end of growing season in temperate vegetation over the Northern Hemisphere for the period 1982–2008. Global change biology, 17(7), 2385-2399. doi: 10.1111/j.1365-2486.2011.02397.x

Jiang, Z., Huete, A. R., Didan, K., & Miura, T. (2008). Development of a 2-band enhanced vegetation index (EVI) without a blue band. Remote Sensing of Environment, 112, 3833–3845. doi: 10.1016/j.rse.2008.06.006.

Jolliffe, I.T. (2002). Principal Component Analysis, Series: Springer Series in Statistics, 2nd ed. Springer, New York, p. 487

Jones, M. O., Kimball, J. S., Jones, L. A., Mcdonald, K. C. (2012). Satellite passive microwave detection of North America start of season. Remote Sensing of Environment. 123, 324-333. doi: 10.1016/j.rse.2012.03.025

Julien, Y., Sobrino, J. A. (2019). Optimizing and comparing gap-filling techniques using simulated NDVI time series from remotely sensed global data. International Journal of Applied Earth Observation and Geoinformation. 76, 93-111. doi: 10.1016/j.jag.2018.11.008

Kassambara, A., & Mundt, F. (2017). Package ‘factoextra’. Extract and visualize the results of multivariate data analyses, 76.

Kaufman, L., Rousseauw, P.J.. (1990). Finding groups in data. An introduction to cluster analysis. Wiley, New York, 1990. doi: 10.1002/9780470316801

Kulkarni, R., Deobagkar, D. and Zinjarde, S. (2018). Metals in mangrove ecosystems and associated biota: A global perspective. Ecotoxicology and Environmental Safety, 153, 215-228. doi: 10.1016/j.ecoenv.2018.02.021.

Lacerda, L.D., Ward, R.D., Godoy, M.D.P., Meireles, A.J.A., Borges, R., Ferreira, A.C. (2021). 20-years cumulative impact from shrimp farming on mangroves of NE Brazil. Frontiers in Forests & Global Change. doi: 10.3389/ffgc.2021.653096

Lewis, M., Pryor,R., Wilking, L. (2011). Fate and effects of anthropogenic chemicals in mangrove ecosystems: A review. Environmental Pollution. 159(10), 2328-2346. doi: 10.1016/j.envpol.2011.04.027

Li, H., Jia, M., Zhang, R., Ren, Y., & Wen, X. (2019). Incorporating the Plant Phenological Trajectory into Mangrove Species Mapping with Dense Time Series Sentinel-2 Imagery and the Google Earth Engine Platform. Remote Sensing, 11(21), 2479. doi: 10.3390/rs11212479

Li, X., Wu, P., Delang, C. O., He, Q., & Zhang, F. (2021). Spatial-temporal variation, ecological risk, and source identification of nutrients and heavy metals in sediments in the peri-urban riverine system. Environmental Science and Pollution Research. doi: 10.1007/s11356-021-15601-y

Lin, S., Li, J., Liu, Q., Li, L., Zhao, J., Yu, W. (2019). Evaluating the Effectiveness of Using Vegetation Indices Based on Red-Edge Reflectance from Sentinel-2 to Estimate Gross Primary Productivity. Remote Sensing. 11(11), 1303. doi: 10.3390/rs11111303

Lletí, R., Ortiz, M., Sarabia, L., & Sánchez, M. (2004). Selecting variables for k-means cluster analysis by using a genetic algorithm that optimises the silhouettes. Analytica Chimica Acta, 515(1), 87-100. doi: 10.1016/j.aca.2003.12.020

Main-Knorn, M., Pflug, B., Louis, J., Debaecker, V., Müller-Wilm, U., & Gascon, F. (2017). Sen2Cor for sentinel-2. In Image and Signal Processing for Remote Sensing XXIII (Vol. 10427, p. 1042704). International Society for Optics and Photonics. doi: 10.1117/12.2278218

Maiti, S., Chowdhury, A. (2013). Effects of Anthropogenic Pollution on Mangrove Biodiversity: A Review. Journal of Environmental Protection. 4(12), 1428-1434. doi: 10.4236/jep.2013.412163

Mandal, M. S., & Hosaka, T. (2020). Assessing cyclone disturbances (1988–2016) in the Sundarbans mangrove forests using Landsat and Google Earth Engine. Natural Hazards, 102(1), 133-150. doi: 10.1007/s11069-020-03914-z

Mandura, A. (1997). A mangrove stand under sewage pollution stress: Red Sea. Mangroves and Salt Marshes. 1, 255–262. doi: 10.1023/A:1009927605517

Marra, G., & Wood, S. N. (2011). Practical variable selection for generalized additive models. Computational Statistics & Data Analysis, 55(7), 2372-2387. doi: 10.1016/j.csda.2011.02.004

McCulley, R., Jobbagy, E., Pockman, W., Jackson, R. (2004). Nutrient uptake as a contributing explanation for deep rooting in arid and semi-arid ecosystems. Oecologia. 141, 620-628. doi: 10.1007/s00442-004-1687-z

Mehlig, U. (2006). Phenology of the red mangrove, Rhizophora mangle L., in the Caeté Estuary, Pará, equatorial Brazil. Aquatic Botany, 84(2), 158-164. doi: 10.1016/j.aquabot.2005.09.007

Nagai, S., Nasahara, K. N., Akitsu, T. K., Saitoh, T. M., & Muraoka, H. (2020). Importance of the Collection of Abundant Ground-Truth Data for Accurate Detection of Spatial and Temporal Variability of Vegetation by Satellite Remote Sensing. Biogeochemical Cycles Geophysical Monograph Series, 223-244. doi: 10.1002/9781119413332.ch11

Naidoo, L., Van Deventer, H., Ramoelo, A., Mathieu, R., Nondlazi, B., Gangat, R. (2019). Estimating above ground biomass as an indicator of carbon storage in vegetated wetlands of the grassland biome of South Africa. International Journal of Applied Earth Observation and Geoinformation. 78, 118-129. doi: 10.1016/j.jag.2019.01.021

Nava-Fuentes, J.C., Arenas, P., Cardoso, F. (2018). Integrated coastal management in Campeche, Mexico: A review after the Mexican marine and coastal national policy. Ocean & Coastal Management. 154, 34-45. doi: 10.1016/j.ocecoaman.2017.12.029

Neina, D. (2019). The role of soil pH in plant nutrition and soil remediation. Applied and Environmental Soil Science. 5794869. doi: 10.1155/2019/5794869

Olivie-Lauquet, G., Gruau, G., Dia, A., Riou, C., Jaffrezic, A., & Henin, O. (2001). Release of trace elements in wetlands: role of seasonal variability. Water research, 35(4), 943-952. doi: 10.1016/S0043-1354(00)00328-6

Otero, V., Kerchove, R. V., Satyanarayana, B., Mohd-Lokman, H., Lucas, R., & Dahdouh-Guebas, F. (2019). An Analysis of the Early Regeneration of Mangrove Forests using Landsat Time Series in the Matang Mangrove Forest Reserve, Peninsular Malaysia. Remote Sensing, 11(7), 774. doi: 10.3390/rs11070774

Pastor-Guzman, J., Atkinson, P., Dash, J., & Rioja-Nieto, R. (2015). Spatiotemporal Variation in Mangrove Chlorophyll Concentration Using Landsat 8. Remote Sensing, 7(11), 14530-14558. doi: 10.3390/rs71114530

Pastor-Guzman, J., Dash, J., Atkinson, P. M. (2018). Remote sensing of mangrove forest phenology and its environmental drivers. Remote Sensing of Environment. 205, 71-84. doi: 10.1016/j.rse.2017.11.009

PEMEX (2018). Anuario Estadístico. (In Spanish) Petróleos Mexicanos.

Pérez, R., Zaldivar, A., Canales, J., Lopez, H., Lopez, J., Merino., M. (2020). Determining hydrological flow paths to enhance restoration in impaired mangrove wetlands. Plos One. 1-20. doi: 10.1371/journal.pone.0227665

Pinheiro, L.M., Agostini, V.O., Lima, A.R.A., Ward, R.D., and Pinho, G.L.L. (2021). The fate of plastic litter within estuarine compartments: an overview of current knowledge for the transboundary issue to guide future assessments. Environmental Pollution. doi: 10.1016/j.envpol.2021.116908

Poszwa, A., Ferry, B., Dambrine, E., Pollier, B., Wickman, T., Loubet, M., Bishop, K. (2004). Variations of bioavailable Sr concentration and Sr-87/Sr-86) ratio in boreal forest ecosystems-role of biocycling, mineral weathering and depth of root uptake. Biogeochemistry. 67, 1-20.

R Core Team (2020). R: A language and environment for statistical computing. R Foundation for Statistical Computing, Vienna, Austria. URL https://www.R-project.org/.

Rahman, A. F., Dragoni, D., Didan, K., Barreto-Munoz, A., & Hutabarat, J. A. (2013). Detecting large scale conversion of mangroves to aquaculture with change point and mixed-pixel analyses of high-fidelity MODIS data. Remote Sensing of Environment, 130, 96-107. doi: 10.1016/j.rse.2012.11.014

Rani, V., Sreelekshmi, S., Preethy, C. M., & BijoyNandan, S. (2016). Phenology and litterfall dynamics structuring Ecosystem productivity in a tropical mangrove stand on South West coast of India. Regional Studies in Marine Science, 8, 400-407. doi: 10.1016/j.rsma.2016.02.008

Reynolds, A.C., Quade, J., Betancourt, J.L. (2012). Strontium isotopes and nutrient sourcing in a semi-arid woodland. Geoderma. 189-190, 574-584. doi: 10.1016/j.geoderma.2012.06.029

Rodriguez-Galiano, V. F., Dash, J., & Atkinson, P. M. (2015). Intercomparison of satellite sensor land surface phenology and ground phenology in Europe. Geophysical Research Letters, 42(7), 2253-2260. doi: 10.1002/2015GL063586

Roerink, G. J., Menenti, M., Verhoef, W. (2000). Reconstructing cloudfree NDVI composites using Fourier analysis of time series. International Journal of Remote Sensing. 21(9), 1911-1917. doi: 10.1080/014311600209814

Shang, R., Liu, R., Xu, M., Liu, Y., Zuo, L., Ge, Q. (2017). The relationship between threshold-based and inflexion-based approaches for extraction of land surface phenology. Remote Sensing of Environment. 199, 167-170. doi: 10.1016/j.rse.2017.07.020

Shiaua, Y.J., Lee, Sh,Ch., Chenc, T.H., Tiand, G., Chiu, Ch.Y. (2017). Water salinity effects on growth and nitrogen assimilation rate of mangrove (Kandelia candel) seedlings. Aquatic Botany. 137, 50-55. doi: 10.1016/j.aquabot.2016.11.008

Simpson, G. L. (2018). Modelling palaeoecological time series using generalised additive models. Frontiers in Ecology and Evolution, 6, 149. doi: 10.3389/fevo.2018.00149

Songsom, V., Koedsin, W., Ritchie R.J., Huete, A. (2019). Mangrove Phenology and Environmental Drivers Derived from Remote Sensing in Southern Thailand. Remote Sensing. 11(8): 955. doi: 10.3390/rs11080955

Songsom, V., Koedsin, W., Ritchie, R. J., & Huete, A. (2021). Mangrove Phenology and Water Influences Measured with Digital Repeat Photography. Remote Sensing, 13(2), 307. doi: 10.3390/rs13020307

Tateishi, R., Ebata, M. (2004). Analysis of phenological change patterns using 1982–2000 Advanced Very High Resolution Radiometer (AVHRR) data. International Journal of Remote Sensing. 25(12), 2287-2300. doi: 10.1080/0143116031000161845

Tecuapetla, T. (2020). geoTS: Methods for Handling and Analyzing Time Series of Satellite Images. R package version 0.1.3. https://CRAN.R-project.org/package=geoTS

Thornton, M.M., Shrestha, R., Wei, Y., Thornton, P.E., Kao, S., Wilson, B.E. (2020). Daymet: Daily Surface Weather Data on a 1-km Grid for North America, Version 4. ORNL DAAC, Oak Ridge, Tennessee, USA. doi: 10.3334/ORNLDAAC/1840

Torres, M.E., McManus, J., Huh, Ch. (2002). Fluid seepage along the San Clemente Fault scarp: basin-wide impact on barium cycling. Earth and Planetary Science Letters. 203, 181-194. doi: 10.1016/S0012-821X(02)00800-2

Turschwell, M. P., Tulloch, V. J., Sievers, M., Pearson, R. M., Andradi-Brown, D. A., Ahmadia, G. N., Brown, C. J. (2020). Multi-scale estimation of the effects of pressures and drivers on mangrove forest loss globally. Biological Conservation. 247, 108637. doi: 10.1016/j.biocon.2020.108637

Upadhyay, V. P., & Mishra, P. K. (2010). Phenology of mangroves tree species on Orissa coast, India. Tropical Ecology, 51(2), 289.

Valderrama-Landeros, L., Flores-Verdugo, F., Rodríguez-Sobreyra, R., Kovacs, J. M., & Flores-De-Santiago, F. (2021). Extrapolating canopy phenology information using Sentinel-2 data and the Google Earth Engine platform to identify the optimal dates for remotely sensed image acquisition of semiarid mangroves. Journal of Environmental Management, 279, 111617. doi: 10.1016/j.jenvman.2020.111617

Veetil, B., Ward, R., Quang, N., Trang, N., Giang, T. (2018). Mangroves of Vietnam: Historical development, current state of research and future threats. Estuarine Coastal Shelf Science. 218: 212-236. doi: 10.1016/j.ecss.2018.12.021

Verger, A., Filella, I., Baret, F., Peñuelas, J. (2016). Vegetation baseline phenology from kilometric global LAI satellite products. Remote sensing of environment. 178, 1-14. doi: 10.1016/j.rse.2016.02.057

Vrieling, A., Meroni, M., Darvishzadeh, R., Skidmore, A. K., Wang, T., Zurita-Milla, R., ... & Paganini, M. (2018). Vegetation phenology from Sentinel-2 and field cameras for a Dutch barrier island. Remote sensing of environment, 215, 517-529. doi: 10.1016/j.rse.2018.03.014

Wafar, S., Untawale, A. G., & Wafar, M. (1997). Litter fall and energy flux in a mangrove ecosystem. Estuarine, coastal and shelf science, 44(1), 111-124. doi: 10.1006/ecss.1996.0152

Wang, D., Wan, B., Liu, J., Su, Y., Guo, Q., Qiu, P., & Wu, X. (2020). Estimating aboveground biomass of the mangrove forests on northeast Hainan Island in China using an upscaling method from field plots, UAV-LiDAR data and Sentinel-2 imagery. International Journal of Applied Earth Observation and Geoinformation, 85, 101986. doi: 10.1016/j.jag.2019.101986

Ward, R., Friess, D., Day, R., Mackenzie, R. (2016). Impacts of Climate Change on Global Mangrove Ecosystems: A Regional Comparison. Ecosystem Health and Sustainability. 2(4): 1-25. doi: 10.1002/ehs2.1211

Wickham, H. (2011). Ggplot2. Wiley Interdisciplinary Reviews: Computational Statistics, 3(2), 180-185. doi: 10.1002/wics.147

Wood, S.N. (2017). Generalized Additive Models: An Introduction with R (2nd edition). Chapman and Hall/CRC.

Wood, S., & Wood, M. S. (2015). Package ‘mgcv’. R package version, 1, 29.

Wu, N., Shi, R., Zhuo, W., Zhang, C., Zhou, B., Xia, Z., . . . Tian, B. (2021). A Classification of Tidal Flat Wetland Vegetation Combining Phenological Features with Google Earth Engine. Remote Sensing, 13(3), 443. doi: 10.3390/rs13030443

Xu, H.M., Tam, N.F.Y., Zan, Q.J., Bai, M., Shin, P.K.S., Vrijmoed, L.L.P., Cheung, S.G., Liao, W.B. (2014). Effects of salinity on anatomical features and physiology of a semi-mangrove plant *Myoporum bontioides*. Marine Pollution Bulletin. 85, 738–746. doi: 10.1016/j.marpolbul.2014.04.003

Younes, N., Joyce, K. E., & Maier, S. W. (2017). Monitoring mangrove forests: Are we taking full advantage of technology? International Journal of Applied Earth Observation and Geoinformation, 63, 1-14. doi: 10.1016/j.jag.2017.07.004

Younes, N., Joyce, K. E., & Maier, S. W. (2021). All models of satellite-derived phenology are wrong, but some are useful: A case study from northern Australia. International Journal of Applied Earth Observation and Geoinformation, 97, 102285. doi: 10.1016/j.jag.2020.102285

Zeng, L., Wardlow, B. D., Xiang, D., Hu, S., & Li, D. (2020). A review of vegetation phenological metrics extraction using time-series, multispectral satellite data. Remote Sensing of Environment, 237, 111511. doi: 10.1016/j.rse.2019.111511

Zhang, X., Friedl, M. A., Schaaf, C. B., Strahler, A. H., Hodges, J. C., Gao, F., Huete, A. (2003). Monitoring vegetation phenology using MODIS. Remote sensing of environment. 84(3), 471-475. doi: 10.1016/S0034-4257(02)00135-9

Zhen, J., Jiang, X., Xu, Y., Miao, J., Zhao, D., Wang, J., . . . Wu, G. (2021). Mapping leaf chlorophyll content of mangrove forests with Sentinel-2 images of four periods. International Journal of Applied Earth Observation and Geoinformation, 102, 102387. doi: 10.1016/j.jag.2021.102387

Zhou, J., Jia, L., Menenti, M. (2015). Reconstruction of global MODIS NDVI time series: Performance of Harmonic ANalysis of Time Series (HANTS). Remote Sensing of Environment. 163: 217-228. doi: 10.1016/j.rse.2015.03.018

Zielinski, M., Dopieralska, J., Krolikowska, S., Walczak, A., Belka, Z. (2021). Mapping of spatial variations in Sr isotope signatures ($^{87}Sr/^{86}Sr$) in Poland-Implications of anthropogenic Sr contamination for archaeological provenance and migration research. Science of the Total Environment. 775, 145792. doi: 10.1016/j.scitotenv.2021.145792

Tables and figures

Table 1. Vegetation indices used in the study.

Name	Formula	Reference
Red Edge Normalized Difference Vegetation Index (NDVIre)	$NDVIre = \frac{NIR_{B8} - rededge_{B5}}{NIR_{B8} + rededge_{B5}}$	Gitleson and Merzylak (1994)
Green Normalized Difference Vegetation Index (GNDVI)	$GNDVI = \frac{NIR_{B8} - Green_{B3}}{NIR_{B8} + Green_{B3}}$	Gitelson et al. (1996)
Two-band Enhanced Vegetation Index (EVI2)	$EVI2 = 2.5\frac{NIR_{B8} - Red_{B4}}{NIR_{B8} + 2.4 * Red_{B4} + 1}$	Jiang et al. (2008)

Table 2. Phenology metrics derived from the HANTS profiles use to characterize phenological patterns in Isla del Carmen mangroves. DOY = Day-of-Year

Phenology parameter	Units	Method
Start-of-season (SoS)	DOY since 1st January, 2019	Maximum change ratio
Length-of-season (LoS)	Number of days between SoS and EoS	Maximum change ratio
Peak-of-season (PoS)	DOY since 1st January, 2019	Timing of the maximum value in the HANTS curve
Seasonal amplitude	Unitless NDVIre values (from 0 to 1)	Difference between the minimum and maximum NDVIre values in the HANTS curve
Growth peak	Unitless NDVIre values (from 0 to 1)	Maximum value of the NDVIre in the HANTS curve during the season

Table 3. PCA results, including loading coefficients, as well as percentage of variance and cumulative percentage of variance explained by each component.

	PC1	PC2	PC3
V (mg/kg)	0.934	0.117	0.294
Cr (mg/kg)	0.243	-0.055	0.915
Co (mg/kg)	0.915	0.240	0.204
Ni (mg/kg)	0.934	-0.036	0.208
Cu (mg/kg)	0	0.974	-0.014
Zn (mg/kg)	0.115	0.954	-0.052
Pb (mg/kg)	0.046	0.987	-0.002
Rb (mg/kg)	0.916	-0.206	0.256
Sr (mg/kg)	-0.561	-0.317	0.461
Ba (mg/kg)	0.064	0.449	0.822
Zr (mg/kg)	0.302	-0.271	0.853
% of variance	41.0	30.4	18.5
Cumulative % of variance	41.0	71.4	89.9

Table 4. Results of pariwise comparison of R^2 fitting performance among three vegetation indices (NDVIre, GNDVI and EVI2) based on one-way ANOVA and Tukey HSD tests. The average R^2 for NDVIre, GNDVI and EVI2 were 0.503, 0.356 and 0.357 respectively.

VI 1	VI 2	Difference	Lower Confidence Interval	Upper Confidence Interval	*p*-Value
GNDVI	EVI2	-0.001	-0.069	0.066	0.998
NDVIre	EVI2	0.145	0.077	0.213	$5.2*10^{-6}$
NDVIre	GNDVI	0.147	0.079	0.0215	$4.2*10^{-6}$

Table 5. Percentage of deviance explained by each variable in single-variable GAMs. Significant contributions of covariates are highlighted in bold, where * indicates significant contribution at the 0.01 level, ** indicates significant contribution at the 0.001 level and *** indicates significant contribution at the 0.0001 level . *Rainfall Jun-Sep* corresponds to the total rainfall during the rainy season (June to September).

Variables	Start of Season (SoS)	Length of Season (LoS)	Peak of Season (PoS)	Seasonal amplitude	Growth peak
Rainfall Jun-Sep	16.8	13.1	10.8	5.76	15
Salinity	**43.9*** **	**26.**5*	**40.2*** **	0	**0**
ORP	0	0.35	0	0.2	15.1
pH	**29.2***	23.5*	**32.1****	7.51	10.4
% Gravel	0	1.43	6.83	0	0
% Sand	7.39	6.81	9.48	0	1.72
% Silt	18.3	14.3	**19***	3.52	6.58
V (mg/kg)	9.56	5.67	0	0	0
Cr (mg/kg)	10.4	11.1	0	0	0
Co (mg/kg)	8.11	8.18	0	0	0
Ni (mg/kg)	7.41	8.78	0	0	1.52
Cu (mg/kg)	**56.9*** **	**56*** **	**19.6***	0	3.49
Zn (mg/kg)	**36***	**32.9***	14.3	2.77	0.78
Pb (mg/kg)	**49.3****	**44.3****	12.2	0	1.4
Rb (mg/kg)	3.73	4.85	0	0	0
Sr (mg/kg)	7.68	10.4	0	10.3	**33.9****
Ba (mg/kg)	17.4	21.2	0	0	5.46
Zr (mg/kg)	9.11	136	3.19	8.01	18.9

Table 6. Description of the four GAMs fitted for Start-os-Season (SoS), Length-of-Season (LoS), Peak-of-Season (PoS) and growth peak, including the percentage of deviance explaine by each model and the adjusted R^2.

Model No.	Phenology metric	Smooth terms	Deviance explained	Adjusted R^2
Model 1	SoS	s(Pb) + s(Cu) + s(Salinity) + s(pH)	92.1%	0.88
Model 2	LoS	s(Cu) + s(Zn) + s(Salinity) + s(pH)	87.7%	0.81
Model 3	PoS	s(Salinity) + s(pH) + s(% Silt)	43.60%	0.4
Model 4	Growth peak	s(Sr)	33.90%	0.29

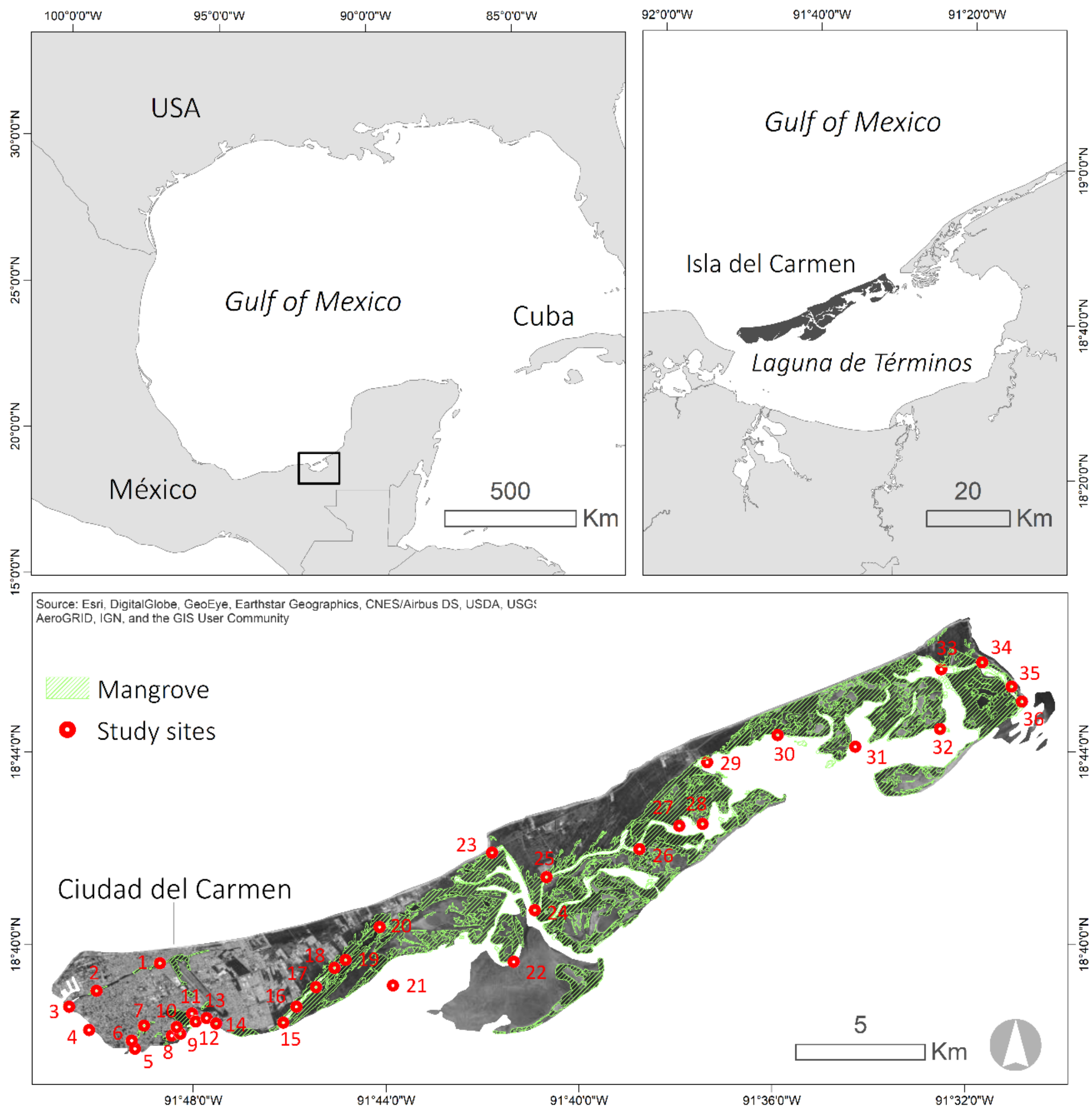

Fig. 1. Location of Isla del Carmen within the Gulf of Mexico (a and b) and location of the thirty-six sampling sites.

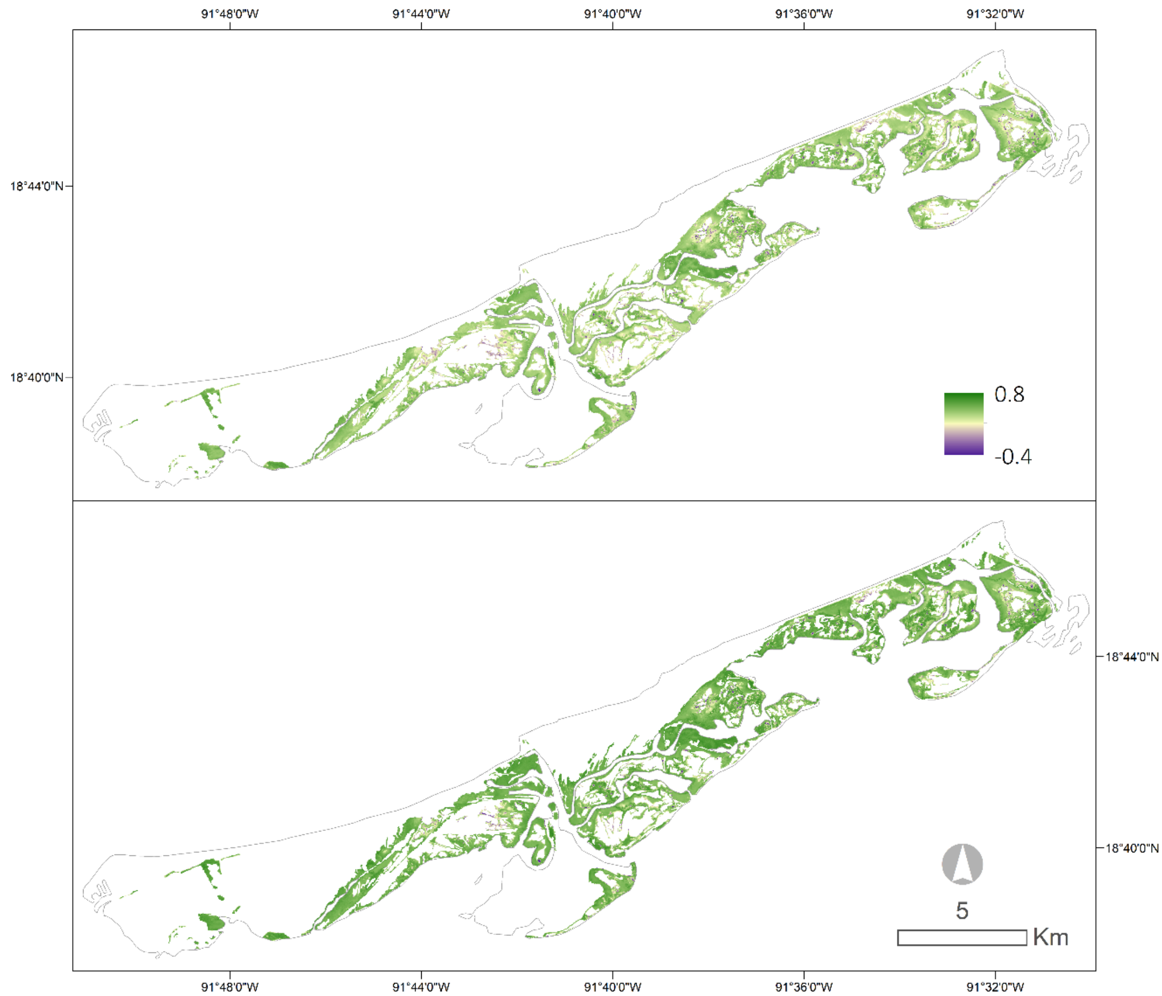

Figure 2. Average NDVIre values between May and July 2019 (A) and between January and February 2020 (B). The NDVIre values were extracted and averaged in Google Earth Engine and correspond to the area defined as mangrove by CONABIO (2013).

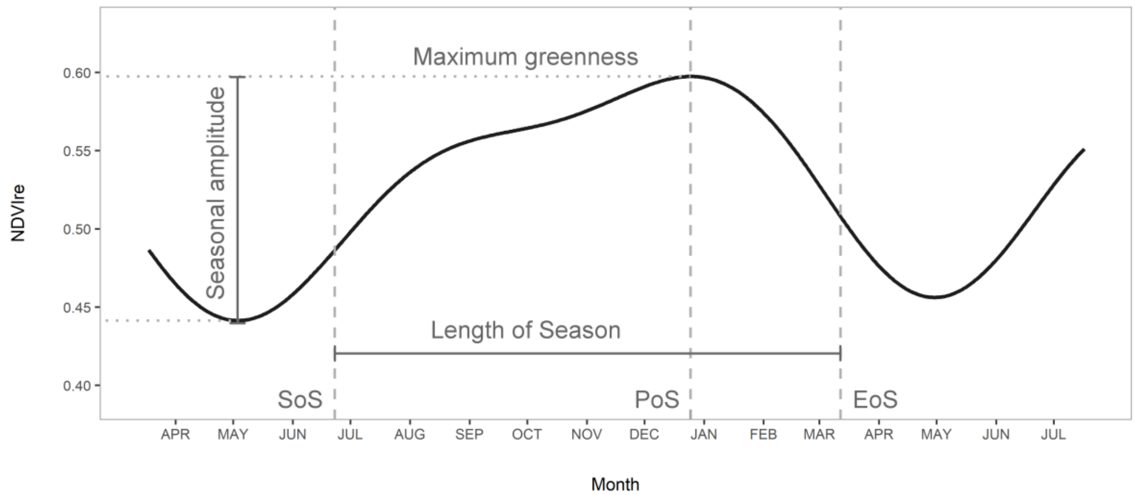

Figure 3. Phenology metrics used to characterize phenological at Isla del Carmen mangroves. The dark grey line represents a typical phenology profile at Isla del Carmen during 2019-2020 season. SoS: Start of season, PoS: Peak of season, EoS: End of season. A description of metrics can be found in table 1.

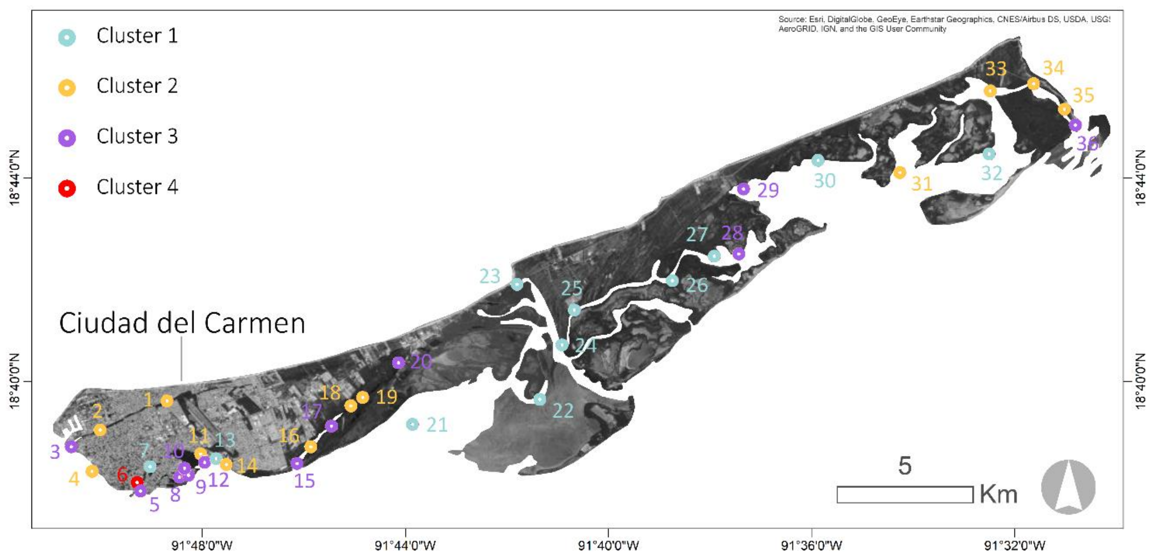

Figure 4. K-means clustering algorithm results, showing the study sites grouped into 4 clusters.

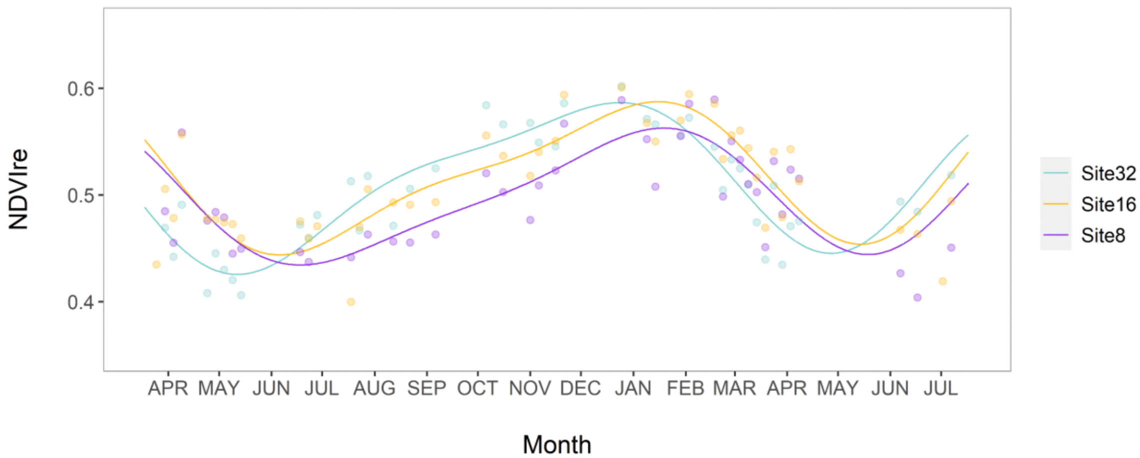

Figure 5. Phenological profiles reconstructed using HANTS algorithm at three study sites. Points show the original values of NDVIre calculated from Sentinel 2 imagery at available dates, whereas the solid lines correspond to the phenology profiles smoothed by the HANTS algorithm.

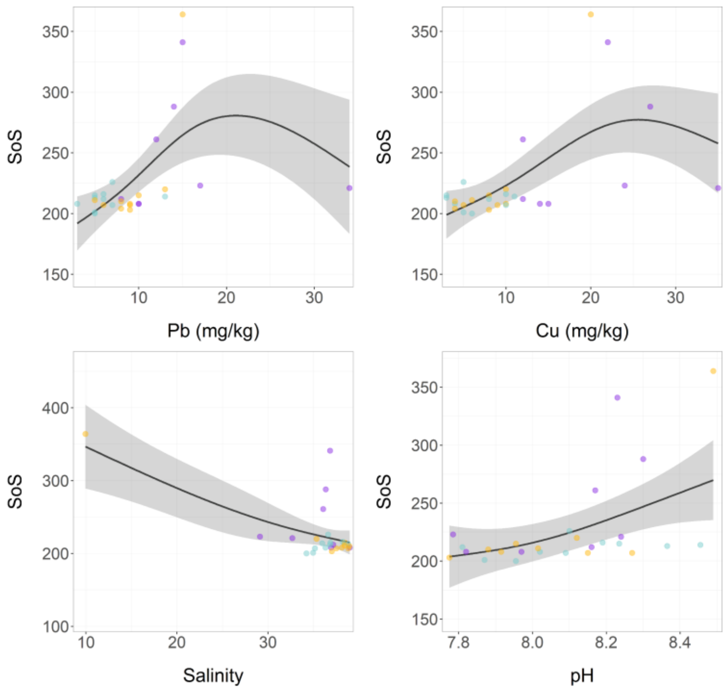

Figure 6. GAMs describing the relationship between the start of season (SoS), two trace elements (Pb and Cu), salinity and pH. Shaded grey areas represent the 95% confidence interval. The fitted curves correspond to model 1. The points are color-coded according to their cluster membership.

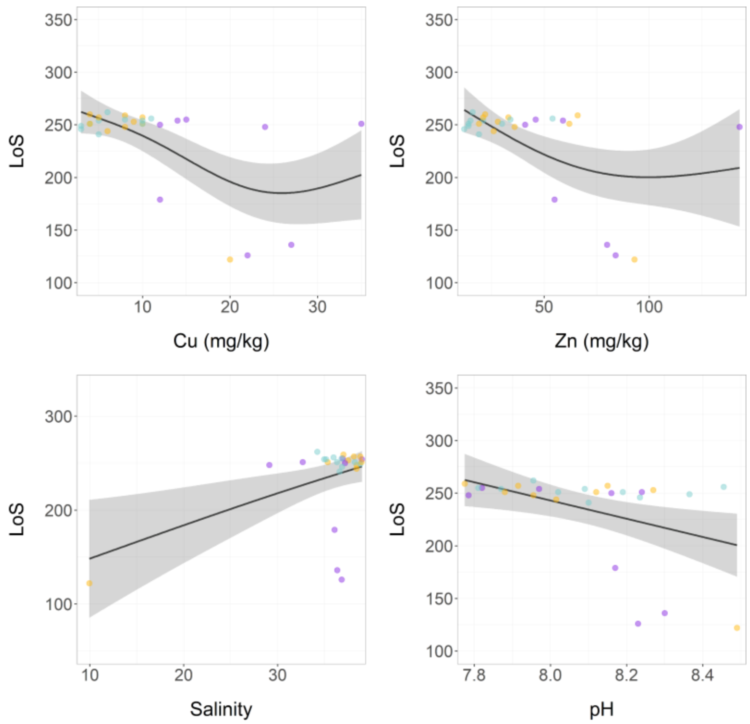

Figure 7. GAMs describing the relationship between the length of season (LoS, difference between start of season and end of season), two trace elements (Cu and Zn), salinity and pH. Shaded grey areas represent the 95% confidence interval. The fitted curves correspond to model 2. The points are color-coded according to their cluster membership.

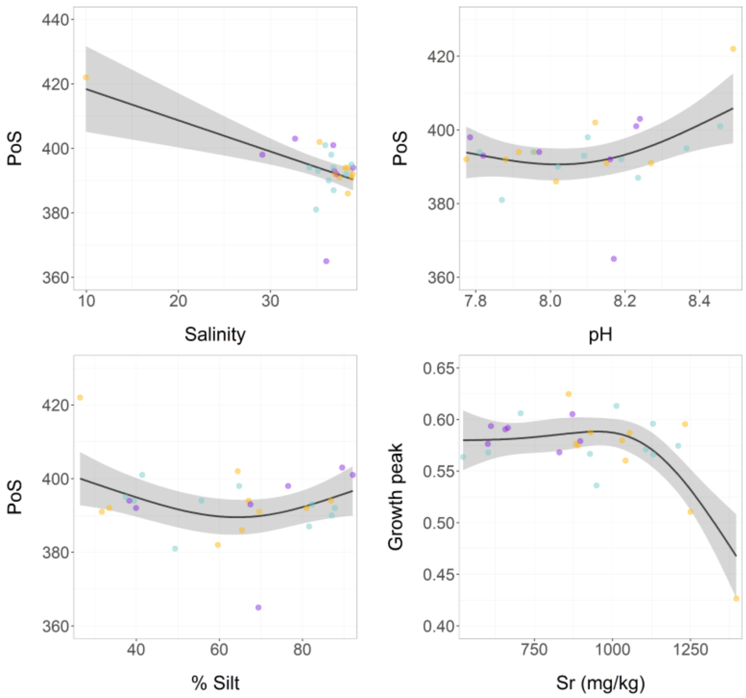

Figure 8. GAMs describing the relationship between peak of season (PoS) and salinity, pH and % silt, and between growth peak (Maximum value of the NDVIre in the phenology curve) and Sr.Shaded grey areas represent the 95% confidence interval. The fitted curves correspond to models 3 and 4. The points are color-coded according to their cluster membership.

Figure 1

fig1.png

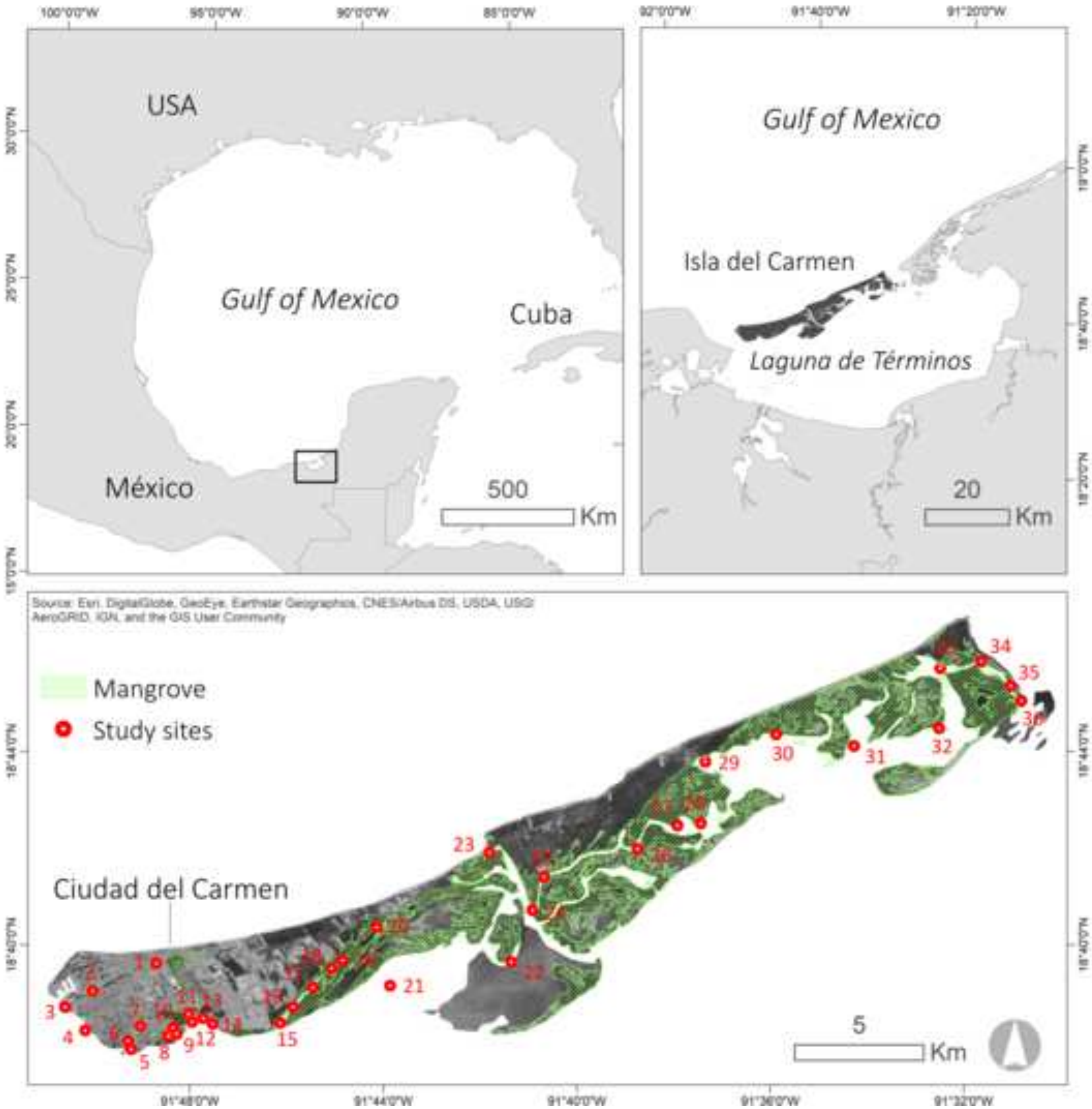

Figure 2

Click here to access/download;Figure;fig2.tif

fig2.png

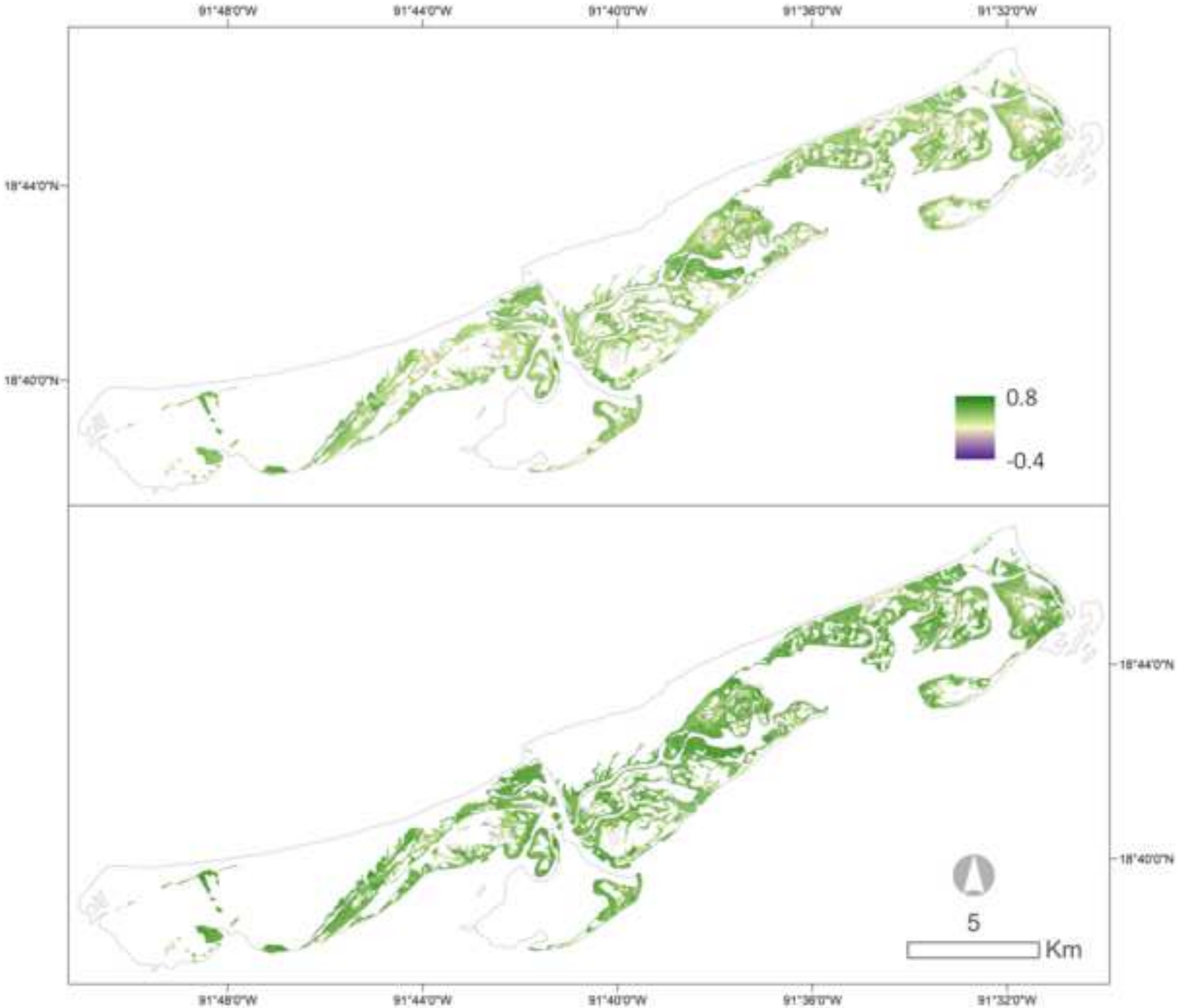

Figure 3

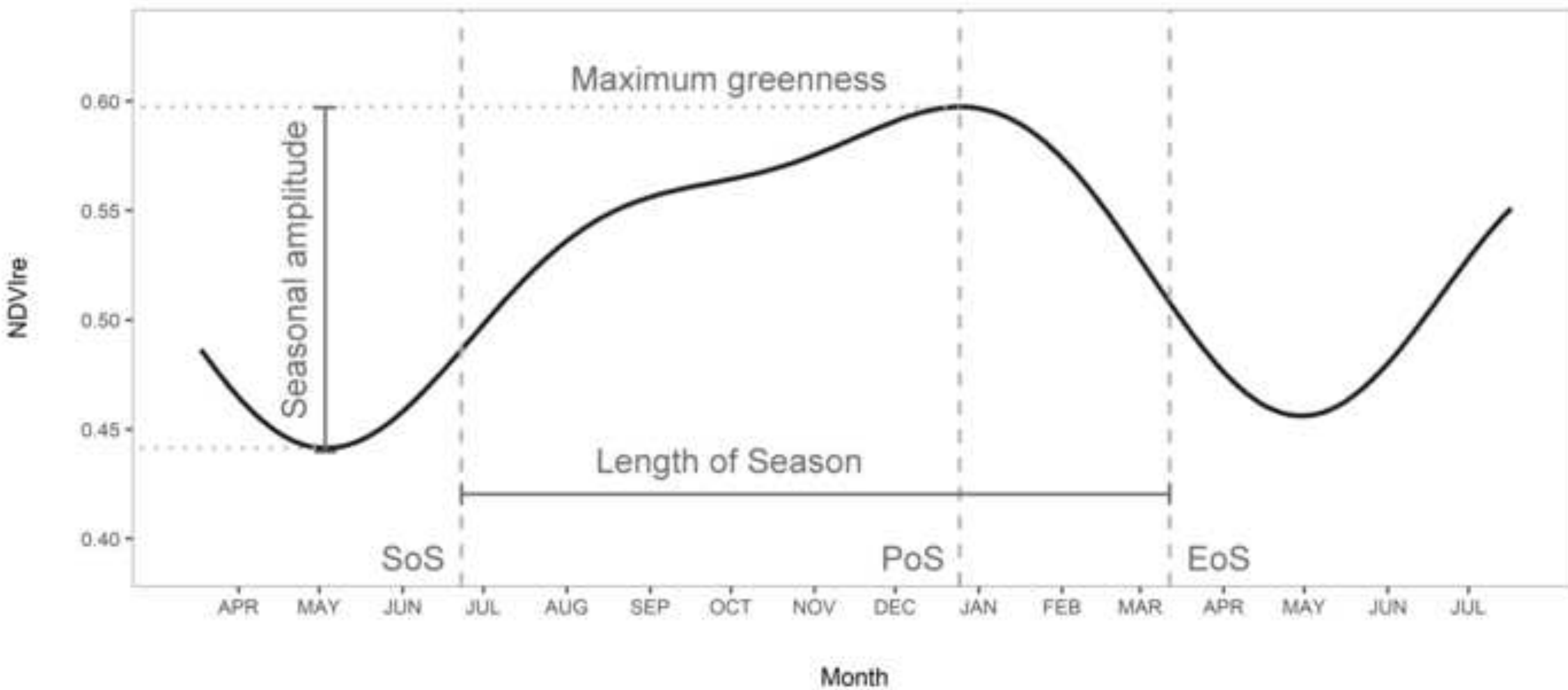
Maximum greenness
Seasonal amplitude
Length of Season
SoS
PoS
EoS
NDVIre
0.60
0.55
0.50
0.45
0.40
APR
MAY
JUN
JUL
AUG
SEP
OCT
NOV
DEC
JAN
FEB
MAR
APR
MAY
JUN
JUL
Month

Figure 4

Click here to access/download;Figure;fig4.tif

fig4.png

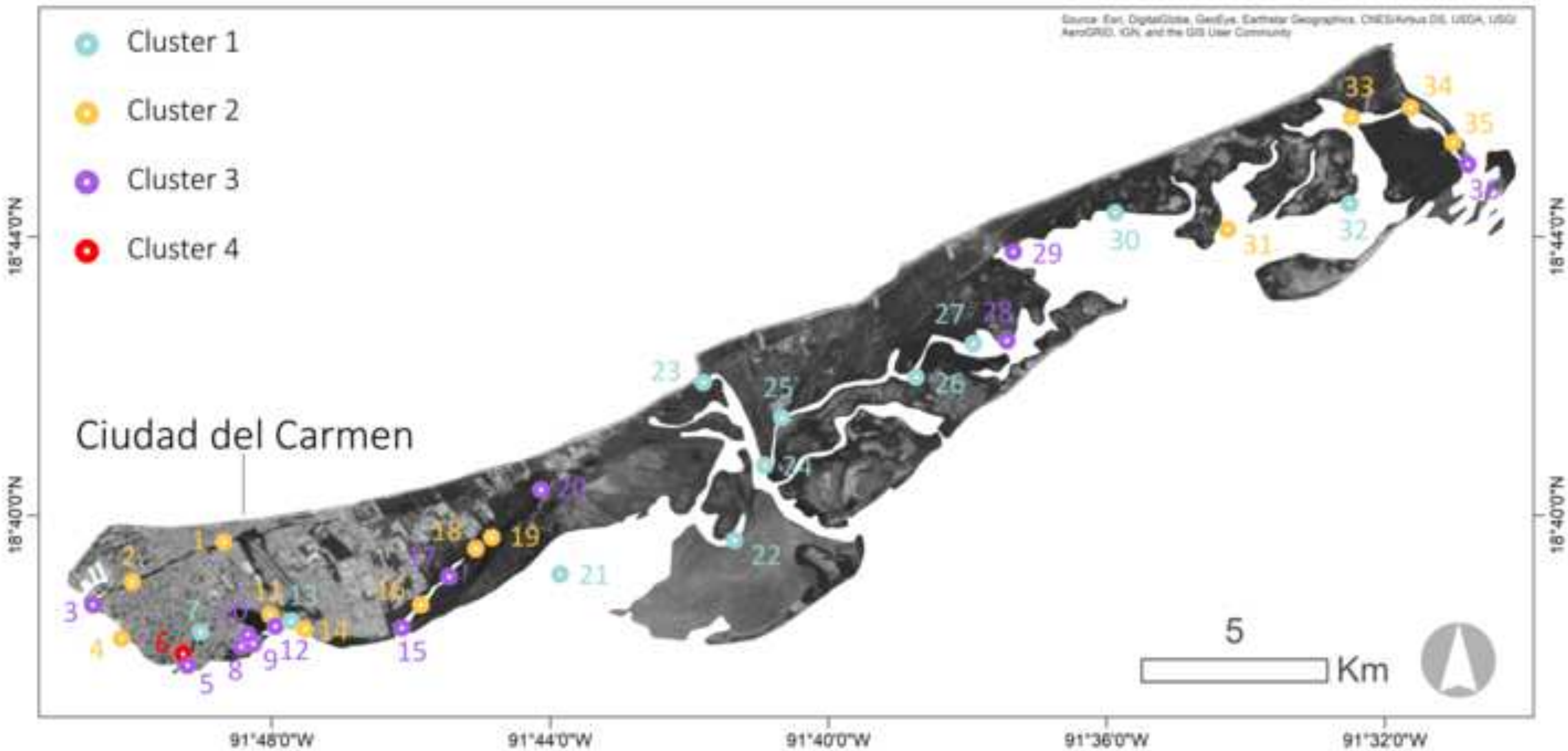

Figure 5

Click here to access/download;Figure;fig5.tif

testfeno2.png

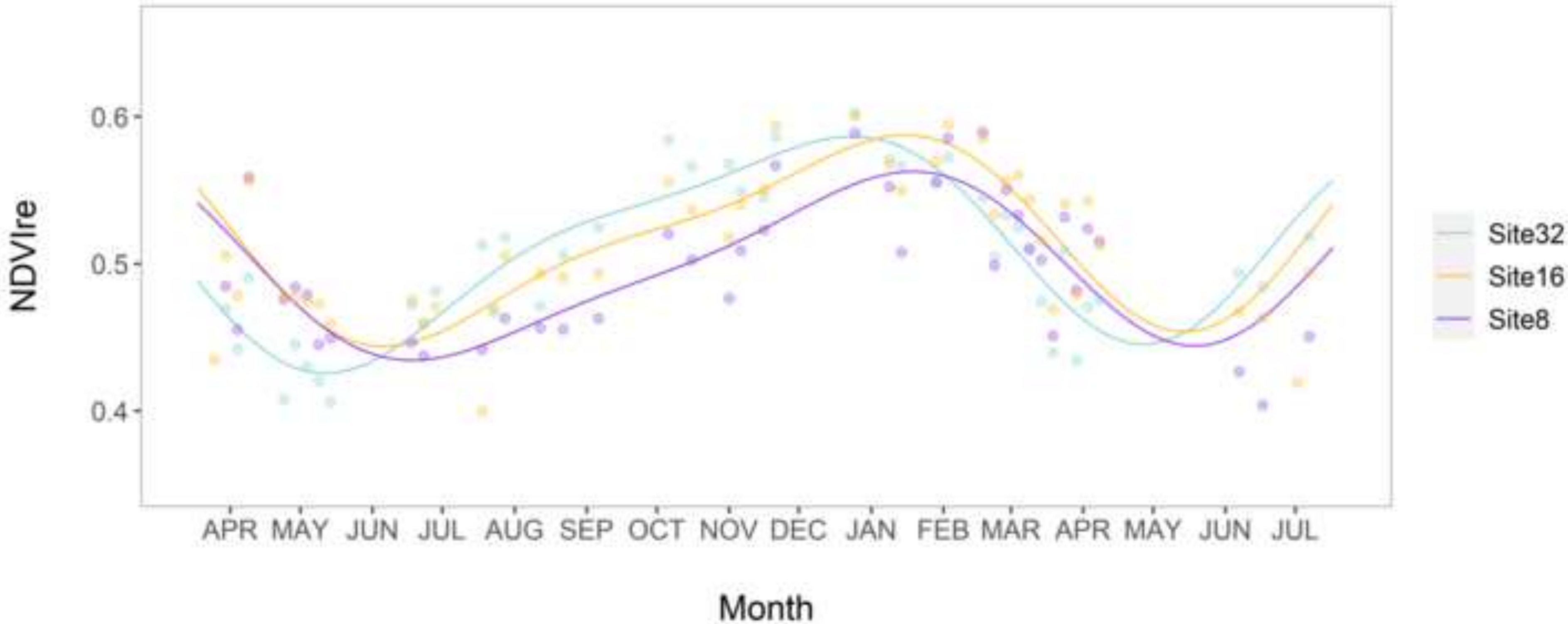

Figure 6

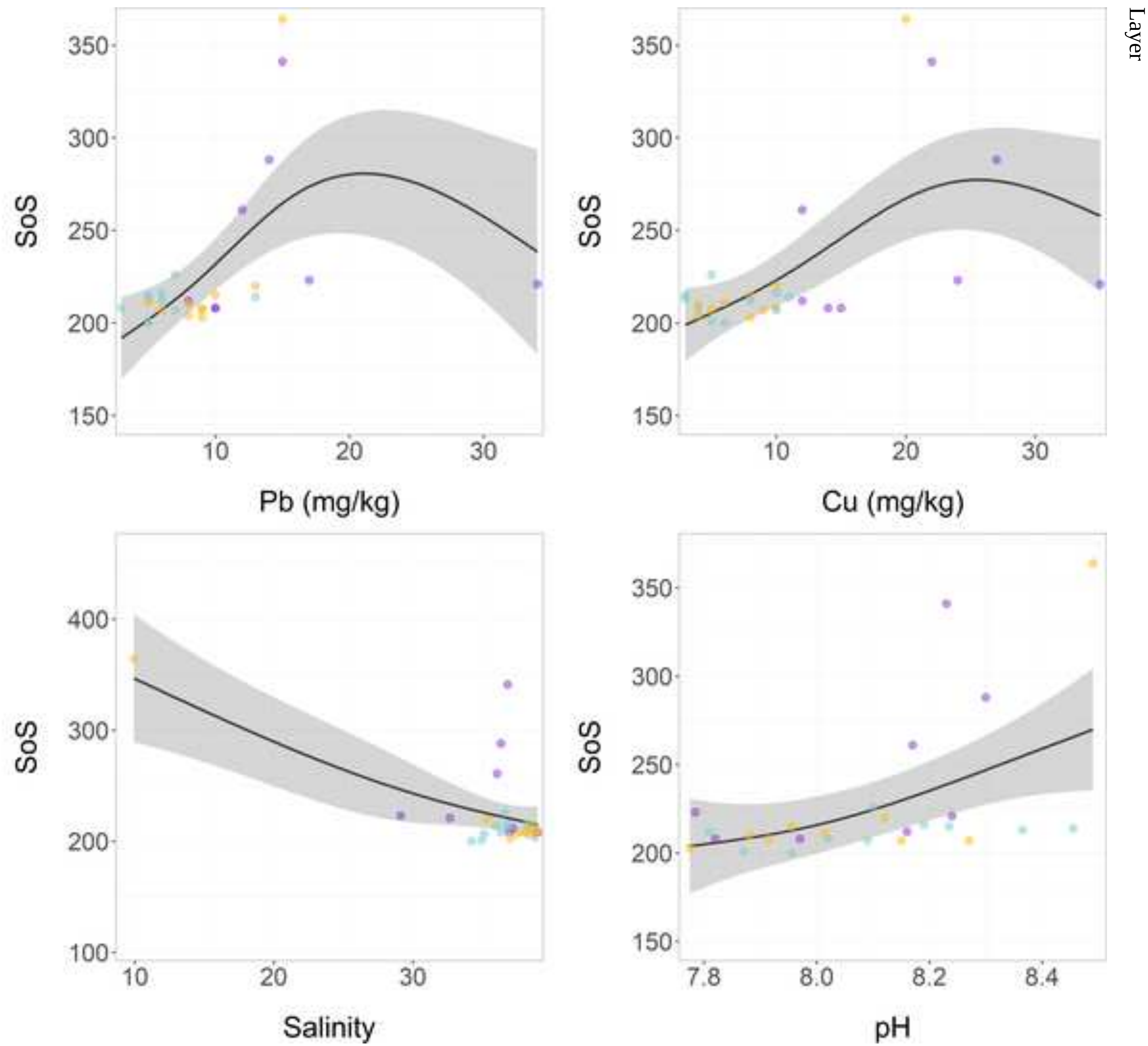
Layer
SoS
Pb (mg/kg)
SoS
Cu (mg/kg)
SoS
Salinity
SoS
pH
350
300
250
200
150
10
20
30
400
100
7.8
8.0
8.2
8.4

Figure 7

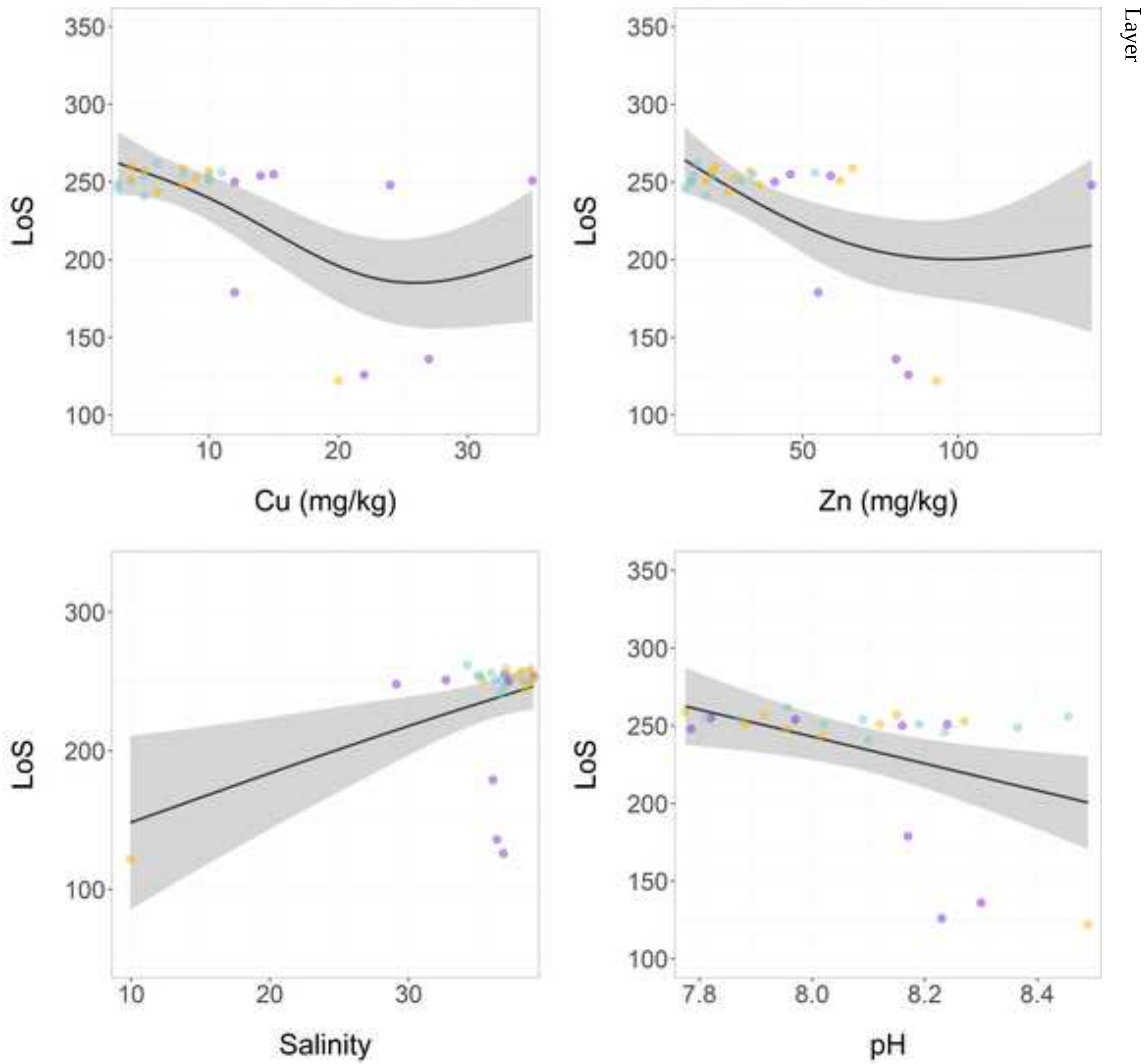
Layer
LoS
350
300
250
200
150
100
10
20
30
Cu (mg/kg)
LoS
50
100
Zn (mg/kg)
LoS
Salinity
LoS
7.8
8.0
8.2
8.4
pH

Figure 8

Click here to access/download;Figure;fig8.tif

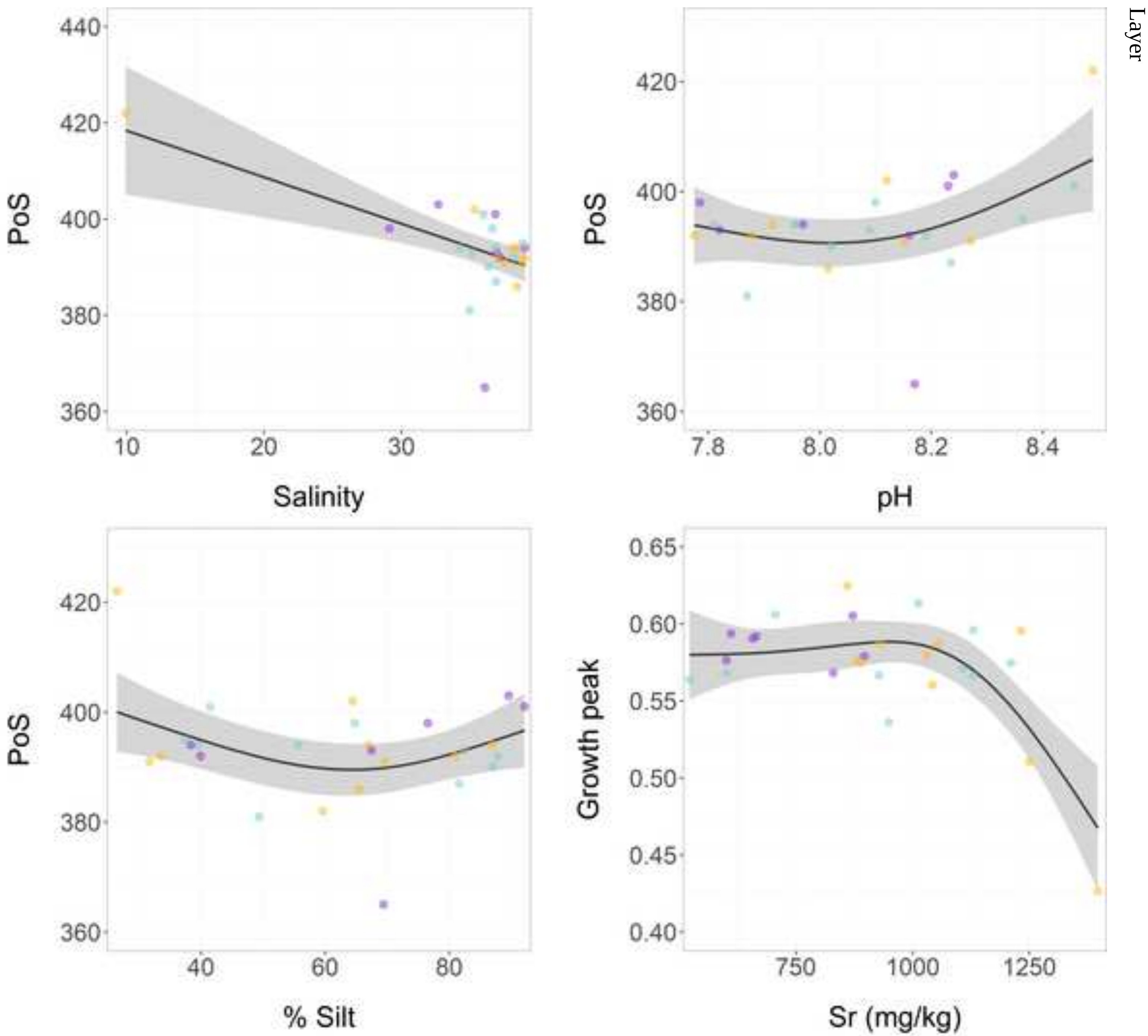

Figure S1

Click here to access/download;Figure;figS1.tif

Layer